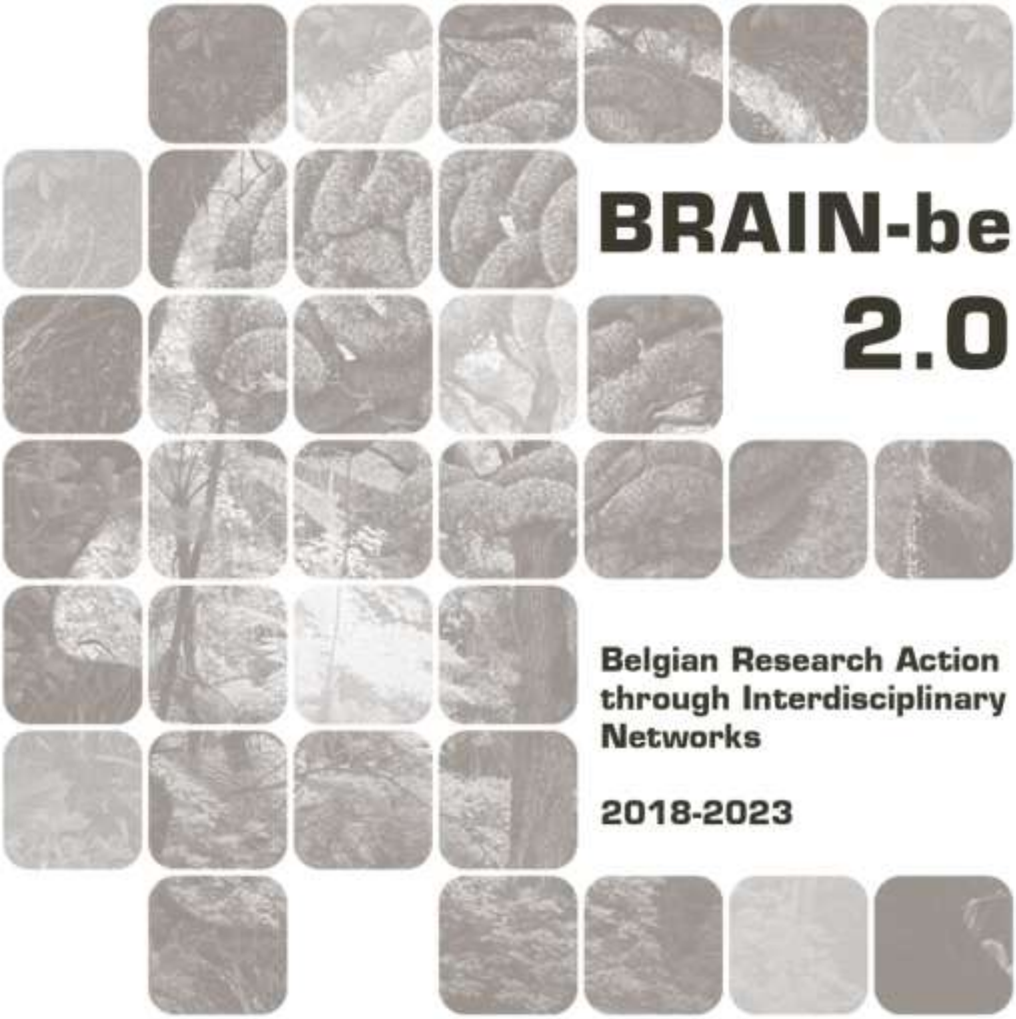

TAPIOWCA

long-Term Assessment, Proxies and Indicators of Ozone and Water vapour changes affecting Climate and Air quality

Daan Hubert (BIRA-IASB) – Arno Keppens (BIRA-IASB) – Catherine Wespes (ULB) – José Granville (BIRA-IASB) – Jean-Christopher Lambert (BIRA-IASB) – Pierre Coheur (ULB)

Pillar 1: Challenges and knowledge of the living and non-living world

belspo .be

BRAIN-be 2.0

Belgian Research Action through Interdisciplinary Networks

2018-2023

NETWORK PROJECT

TAPIOWCA

long-Term Assessment, Proxies and Indicators of Ozone and Water vapour changes affecting Climate and Air quality

Contract - B2/223/P1/TAPIOWCA

FINAL REPORT

PROMOTORS: Daan Hubert (Koninklijk Belgisch Instituut voor Ruimte Aeronomie, BIRA-IASB)
Pierre Coheur (Université Libre de Bruxelles, ULB)

AUTHORS: Daan Hubert (BIRA-IASB)
Arno Keppens (BIRA-IASB)
José Granville (BIRA-IASB)
Jean-Christopher Lambert (BIRA-IASB)
Catherine Wespes (ULB)
Pierre Coheur (ULB)

BIRA•IASB ULB

belspo .be

Published in 2026 by the Belgian Science Policy Office
WTCIII
Simon Bolivarlaan 30 bus 7
Boulevard Simon Bolivar 30 bte 7
B-1000 Brussels
Belgium
Tel: +32 (0)2 238 34 11
http://www.belspo.be
http://www.belspo.be/brain-be

Contact person: Corinne Lejour
Tel: +32 (0)2 238 34 91

Hubert, Daan, Keppens, Arno, Wespes, Catherine, Granville, José, Lambert, Jean-Christopher and Coheur, Pierre. **long-Term Assessment, Proxies and Indicators of Ozone and Water vapour changes affecting Climate and Air quality**. Final Report. Brussels: Belgian Science Policy Office 2026 – 50 p. (BRAIN-be 2.0 - (Belgian Research Action through Interdisciplinary Networks))

TABLE OF CONTENTS

ABSTRACT

Ozone and water vapour are central to climate change, air quality and surface ultraviolet radiation, environmental challenges with far-reaching effects on societies and ecosystems. Despite major international efforts, long-term changes remain uncertain for stratospheric water vapour and for ozone in the troposphere and lower stratosphere. TAPIOWCA addressed several challenges that limit current scientific assessments. First, the project improved satellite records of tropospheric ozone. Measurements from three IASI sensors were combined, and results from a IASI retrieval setup with improved stability was further consolidated. Harmonisation of sixteen satellite ozone records showed that differences in tropospheric column definition are not the main cause of inter-dataset discrepancies. Second, TAPIOWCA extended statistical models to better capture observed variability. Additional regression terms for ozone precursor emissions and for stratosphere-troposphere exchange were found to improve tropospheric ozone trend analyses. The response time of ozone to El Niño-Southern Oscillation events was also mapped, although its impact on lower stratospheric ozone trends remains modest. Finally, TAPIOWCA reassessed present-day conditions and past changes in ozone and water vapour across the troposphere and stratosphere. The project made a central contribution to the second TOAR assessment, supporting high-confidence evidence of increasing tropospheric ozone in most of the Northern Hemisphere until the COVID-19 pandemic and enabling improved maps of the present-day mean state and seasonal cycle. While 1992-2004 trends in stratospheric water vapour remain uncertain in the middle and upper stratosphere, agreement improves markedly for trends since 2005. The sign of observed water vapour trends is consistent with expectations from a warming troposphere and changing cold point temperatures. Overall, TAPIOWCA has provided robust observational records, methods and results in support of current and upcoming environmental assessments.

Keywords: satellite observations, climatology, interannual variability, long-term trends, tropospheric ozone, stratospheric ozone, stratospheric water vapour.

1 INTRODUCTION

Ozone and water vapour play fundamental roles in the Earth's atmosphere and are deeply involved in several major environmental concerns: air quality, climate change and ultraviolet radiation. Ozone in the troposphere causes respiratory problems, reduces ecosystem productivity and acts as a greenhouse gas. Ozone in the stratosphere, on the other hand, protects life at the surface from harmful solar UV-B radiation, determines the thermal structure and radiative balance in the stratosphere, and affects surface temperatures as well. Water vapour is the single most important natural greenhouse gas in the atmosphere and provides a strong positive feedback to anthropogenic climate forcing from carbon dioxide; its tropospheric abundance determines cloud formation and the water cycle.

In order to improve our understanding and, ultimately, future projections of the environmental impact of atmospheric ozone and water vapour, the research community relies, a.o., on accurate long-term measurements (so-called climate data records, CDRs) and on time series analyses which disentangle and quantify the different modes of climate variability and long-term trends in the Earth system. Identifying where changes in the atmosphere occur is of prime importance since these determine the nature and scale of the long-term effects (WMO, 2022; IPCC, 2021; and references therein).

Several international initiatives and projects, supported by e.g. IGAC (International Global Atmospheric Chemistry project), APARC (Atmospheric Processes And their Role in Climate) and WMO's Global Atmospheric Watch (GAW), have been launched to improve the observational constraints on the present-day distribution, its interannual variability and long-term changes of ozone and water vapour. Despite these efforts, the latest international assessments (TOAR-I, 2019; IPCC, 2021; WMO, 2022) conclude that the level of confidence in long-term trends of stratospheric water vapour (low), lower stratospheric ozone (medium) and tropospheric ozone (medium) remains below par. This is a consequence of common challenges for the involved research communities: (a) measurement uncertainty at the level of single sensors and of merged data records, and (b) incomplete attribution of natural variability.

TAPIOWCA (for long-Term Assessment, Proxies and Indicators of Ozone and Water vapour changes affecting Climate and Air quality) targeted several specific details of above challenges, generating improved tropospheric ozone data records and developing improved regression methods. Together this allowed us to obtain more robust and more constrained estimates of past and current changes in ozone and water vapour at various temporal and spatial scales, and to discriminate between natural and anthropogenic forcings. Data records and research findings developed within the TAPIOWCA project were presented across different research communities and contribute to ongoing assessments by TOAR, WMO and IPCC.

2 STATE OF THE ART AND OBJECTIVES

Recent assessments of long-term (satellite) climate data records (CDRs) by WMO, TOAR and IPCC report insufficient confidence in several key trend estimates (TOAR-I, 2019; IPCC, 2021; WMO, 2022): low confidence for stratospheric water vapour, and only medium confidence for lower stratospheric ozone and tropospheric ozone. This limits the reliability of conclusions about atmospheric change and its implications for climate, air quality and ultraviolet radiation. The main open challenges are methodological and observational.

First, measurement uncertainties remain incompletely characterised, especially for tropospheric composition observed from space. Different instruments vary in vertical sensitivity, vertical resolution, spatial coverage and sampling, while definitions of the tropopause and tropospheric ozone content are not yet fully harmonised (Gaudel et al., 2018; Tarasick et al., 2019; Keppens et al., 2019). These differences can lead to inconsistent estimates of ozone distributions and trends.

Second, the construction of multi-decadal CDRs from multiple sensors introduces additional uncertainty. Data merging methods attempt to account for instrument biases and sampling differences, but bias-correction schemes have limitations, particularly when biases vary over time. As a result, the stability and coherence of merged records can depend strongly on the selected input datasets and merging assumptions. Remaining discrepancies have been reported for both stratospheric water vapour CDRs (Hegglin et al., 2014; Hurst et al., 2016, Khosrawi et al., 2018) and lower-stratospheric ozone CDRs (e.g., Hubert et al., 2016; SPARC/IO3C/GAW, 2019; Godin-Beekmann et al., 2022), while systematic merging of tropospheric ozone profile records remains less mature.

Third, interannual variability can obscure small decadal trends. Processes such as the seasonal cycle, El Niño Southern Oscillation (ENSO), Quasi-Biennial Oscillation (QBO) and solar variability must be represented carefully in regression analyses, but available proxy time series are imperfect and atmospheric responses may occur with spatially variable time lags (Damadeo et al., 2014; de Laat et al., 2015; Diallo et al., 2018). These time lags are not yet well characterised, despite their potential impact on trend estimates and uncertainties.

At the same time, several emerging opportunities make progress possible. Tropospheric ozone CDRs are available with latitude-longitude resolution, allowing spatial patterns to be analysed from regional to global scales. In addition, mature CDRs are becoming available for multiple Essential Climate Variables. Assessing consistency between variables, such as ozone and water vapour, offers a route toward more integrated Earth-system trend detection, improved evaluation of climate models and stronger attribution of observed atmospheric changes to climate forcing.

These outstanding challenges and emerging opportunities were translated into the following research objectives for TAPIOWCA

(RO1) Improve (the understanding of) the agreement between tropospheric ozone CDRs (a) by homogenising IASI measurements, and, (b) by applying a harmonisation scheme that corrects for differences in the vertical perception of all major CDRs.

(RO2) Characterise remaining differences between tropospheric ozone CDRs and identify possible causes.

(RO3) Using multiple linear regression (MLR) techniques, investigate whether changes in ozone precursor concentrations or in exchanges between stratosphere and troposphere can explain (part of) the trend in tropospheric ozone.

(RO4) Improve the representation of interannual variability by optimising the time lag of the response of ozone to natural processes, characterise its spatial structure and its impact on the regressed parameters and uncertainties.

(RO5) Based on multiple CDRs used widely in the community, assess the present-day mean state, the interannual variations and the long-term trend of ozone in the troposphere & stratosphere, and, of water vapour in the upper troposphere and stratosphere.

(RO6) Adopt a systematic and comprehensive approach across the project, in order to reduce uncertainty and to maximise robustness of the project’s assessments. Do this by intercomparing different CDRs, in troposphere and stratosphere, and by exploring relations between ozone and water vapour.

3 METHODOLOGY AND SCIENTIFIC RESULTS

This section details the research objectives, data sets, methods and scientific results of each TAPIOWCA work package. Section 4 provides a scientific summary and lists recommendations from this work.

3.1 WP 1: Homogenisation of IASI tropospheric ozone data records

The main goal of WP 1 is the release of homogenised IASI tropospheric ozone data records, previous versions of which suffered from inhomogeneities resulting from updates in Level-1 and Level-2 algorithms.

3.1.1 Global processing of homogenised IASI-A/B/C data

The first task of WP 1 consists in the production and delivery of merged tropospheric ozone (TrO3) columns from the three IASI instruments (IASI-A/B/C) into a homogenised dataset in terms of FORLI retrieval algorithm.

Indeed, the three IASI instruments provide high-quality calibrated radiances, which have proven to be extremely stable over the duration of the mission, leading to remarkable consistency between IASI-A, -B and -C (Chinaud et al., 2019). It allows us to consider combining the three IASI TrO3 datasets and provide a quite unique IASI dataset for long-term ozone assessments (IGAC TOAR, WMO/UNEP).

The homogenised IASI-A/B/C dataset, created as part of TAPIOWCA, consists of gridded daily merged IASI TrO3 columns in 1° latitude x 1° longitude bins from 90°S to 90°N and from 180°W to 180°N. Two tropospheric columns are provided: from surface to 6 km altitude and from surface to the thermal tropopause. They combine data retrieved from the three IASI sensors using the method described below.

Methods

The IASI merged Level-3 TrO_3 column dataset generated for TAPIOWCA (IASI L3 ULB-LATMOS MG-FORLI-TAP, version 1.0) is produced at ULB-LATMOS for the period 2008-2022, running a merging scheme on daily Level-2 IASI/Metop-A (1 January 2008 to 19 September 2019), -B (8 March 2013 to 31 December 2023) and -C (20 September 2019 to 31 December 2023) TrO_3 columns integrated from IASI Level-2 ozone profiles reprocessed at ULB using the latest version of the FORLI-O3 v20191122 retrieval algorithm (Fast Optimal Retrieval on Layers for IASI; Hurtmans et al., 2012). The reprocessing of IASI L2 O_3 profiles over the entire duration of the IASI mission with the latest release of FORLI-O_3 assures the consistency between the three IASI datasets. The general retrieval quality flag as recommended for the use of the standard IASI L2 O_3 profiles has been applied on the three reprocessed IASI L2 O_3 profile datasets before merging the corresponding integrated L2 TrO_3 columns.

IASI L3 MG-FORLI-TAP is created by a weighted averaging of the L2 TrO_3 columns (x_i) from individual IASI-A, -B and -C instruments assigned to the 1°x1° bins. The weights used for the averaging are the reciprocal square of the total retrieval random errors (σ_i, i.e. measurement and smoothing errors) associated with the retrieved TrO_3 column, as reported by the FORLI-O3 (v20191122) retrieval algorithm. The random uncertainty (σ) of the weighted mean is calculated through error propagation as the reciprocal sum of all the individual weights assigned to a cell. The weighted average ozone value ($\bar{x}_w$) and its associated error estimate (σ) in a specific column and in a Level-3 grid cell are therefor calculated as follows

$$\bar{x}_w = \frac{\sum_i \frac{x_i}{\sigma_i^2}}{\sum_i \frac{1}{\sigma_i^2}} \qquad \text{and} \qquad \sigma^2 = \frac{1}{\sum_i \frac{1}{\sigma_i^2}}.$$

Results

Figure 1 shows an example of the daily distribution (30 March 2018) of tropospheric ozone columns from IASI-A L2 (left panel) and merged IASI-A and -B L3 (right panel). It clearly highlights the benefit of the merged product in terms of spatio-temporal coverage. Another important feature of the merged TrO3 product is the decrease of the corresponding random uncertainty, on average by a factor of 1.5-2, in comparison with L2 retrieval error. It reflects all the individual weights assigned to a 1°x1° grid cell.

The IASI L3 ULB-LATMOS MG-FORLI-TAP (V1.0) data product processed at ULB-LATMOS is stored in the BIRA-IASB data repository (https://doi.org/10.18758/70hjwnl0) as NetCDF-4 files (one file per day), which can be read with standard software packages.

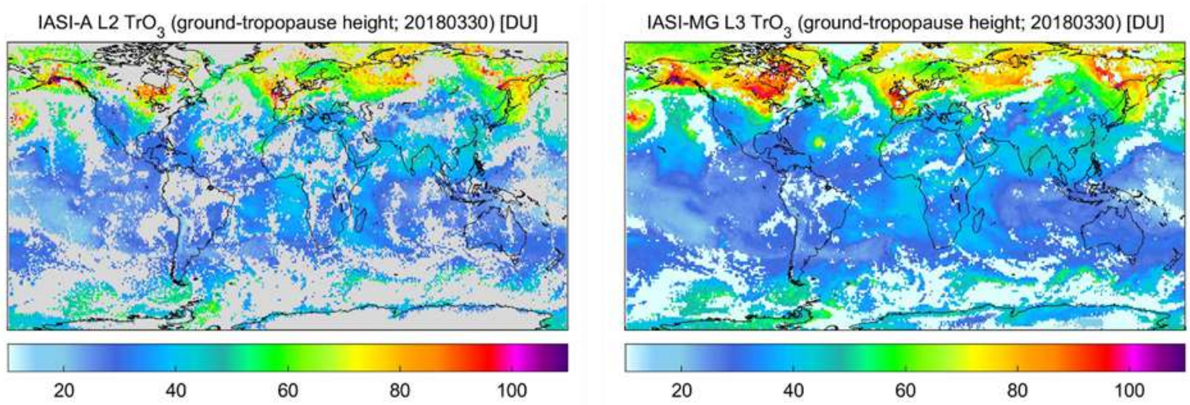

Figure 1. Tropospheric O3 column (surface to tropopause; in Dobson Units, DU) on a daily 1° x 1° grid (30 March 2018) from IASI-A L2 (left panel) and merged IASI-A and -B L3 (right panel).

3.1.2 Processing IASI-A ozone with improved FORLI-clim over selected sites

The second task of WP 1 consists in the release of a IASI O3 Climate Data Record (CDR) dataset, which is fully homogeneous in terms of Level-1C IASI radiances, of Level-2 inputs used in the FORLI-O3 algorithm and of FORLI-O3 version.

Initially, a climate version of FORLI called "FORLI-clim" was set up at ULB to ingest EUMETSAT homogeneous reprocessed L1C IASI radiances and homogeneous L2 temperature and humidity profiles taken from the ERA-5 reanalysis. This configuration was tested for a restricted number of selected stations due to computing constraints. FORLI-clim provided real improvements with respect to the correction of artificial drift caused by updates in the EUMETSAT L1 and L2 algorithms, which paved the way for the development of a homogeneous IASI L2 O3 product on a global scale: IASI L2 ULB-LATMOS O3 CDR product.

Methods

The IASI Level-2 O3 CDR product has been generated at EUMETSAT using the FORLI-O3 v20151001 retrieval algorithm (Hurtmans et al., 2012). FORLI relies on a fast radiative transfer and retrieval methodology based on the Optimal Estimation Method (Rodgers, 2000). It adjusts profile in layer partial columns applying multiplicative factors on an a priori profile used as reference. The IASI L2 O3 CDR product is a profile retrieved on 40 layers between the surface and 40 km, with an extra layer from 40 to 60 km, the top of the atmosphere (TOA). It is provided along with associated averaging kernels and retrieved total errors on the same vertical grid. The height of the thermal tropopause is also provided, allowing users to calculate TrO3 columns by integrating O3 profiles from the surface to the tropopause.

The IASI L2 O3 CDR dataset is processed at EUMETSAT for the period 2008-2023 running FORLI-O3 on homogeneous daily L1C radiances from two of the three IASI instruments: IASI/Metop-A from 2008 to 2019 (reprocessed L1C until December 2016 – doi:10.15770/EUM_SEC_CLM_0014 – and operational L1C onwards, no doi) and IASI/Metop-B (operational L1C; no doi) from 2020 to 2023, and ingesting, as inputs, IASI L2 temperature and humidity profiles that were homogeneously reprocessed by EUMETSAT (Release 1 IASI L2 CDR). The IASI L2 O3 CDR is produced for twice daily measurements, but due to computing constraints only for 3-4 pixels out of 10.

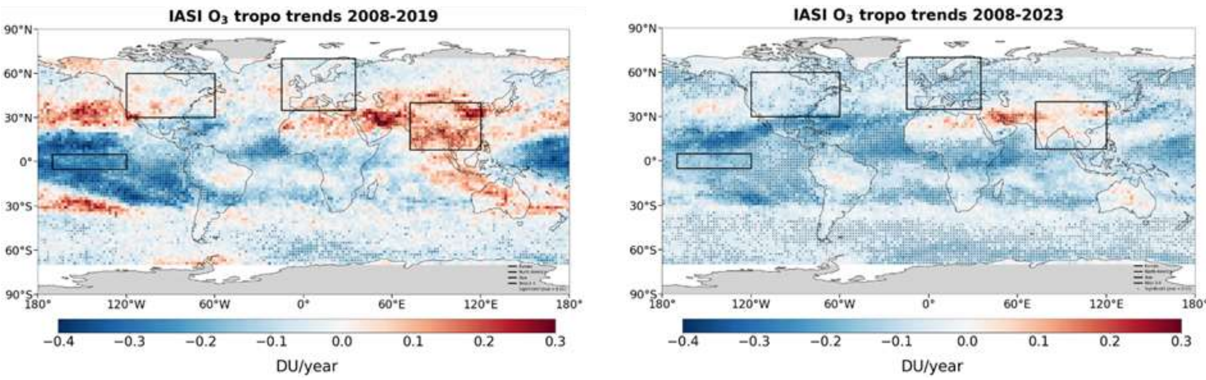

Figure 2. Spatial distribution of tropospheric ozone trends (DU per year) derived from the L2 IASI TrO3 CDR product before the COVID-19 pandemic (2008-2019) and including the pandemic (2008-2023). Dots indicate trends with 95% confidence. The black rectangles indicate the boundaries of four regions shown in **Figure 3**. Figure from Boynard et al. (2025).

Results

The quality of the IASI L2 TrO3 CDR product was assessed by Boynard et al. (2025), through validation against data by the Cross-track Infrared Sounder (CrIS) and ozonesondes. Both comparisons show good agreement for tropospheric ozone with a bias up to 10% in mid-latitudes and polar regions. The study also highlights the contribution of the IASI TrO3 CDR product to a long-term ozone assessment. **Figure 2** presents the tropospheric O3 trends inferred from IASI L2 TrO3 CDR over two different periods: the first stops before the COVID lockdown (2008-2019) and the second covers the whole IASI period (2008-

2023). The effect of the lockdown on the TrO3 trends is clearly visible, especially in the Northern Hemisphere (NH), where TrO3 trends are changing from positive to negative due to a reduction in ozone precursors (NOx and VOCs) and, hence, to a decrease in ozone production. This drop in TrO3 is clearly visible in monthly IASI TrO3 anomaly time series (**Figure 3**) for different latitude bands and regions (see **Figure 2** for the definition of the regions): the negative TrO3 anomalies starting in 2020 across most of the regions (except over Asia and the Nino 3.4 region) continue until 2023.

The EUMETSAT IASI L2 O3 CDR has been distributed via EUMETCast (in NetCDF format) using principal component compression (PCC). The files are then reformatted by LATMOS in NetCDF format after data reconstruction and are distributed by AERIS (IASI-A https://doi.org/10.25326/806, IASI-B https://doi.org/10.25326/807, IASI-C https://doi.org/10.25326/805).

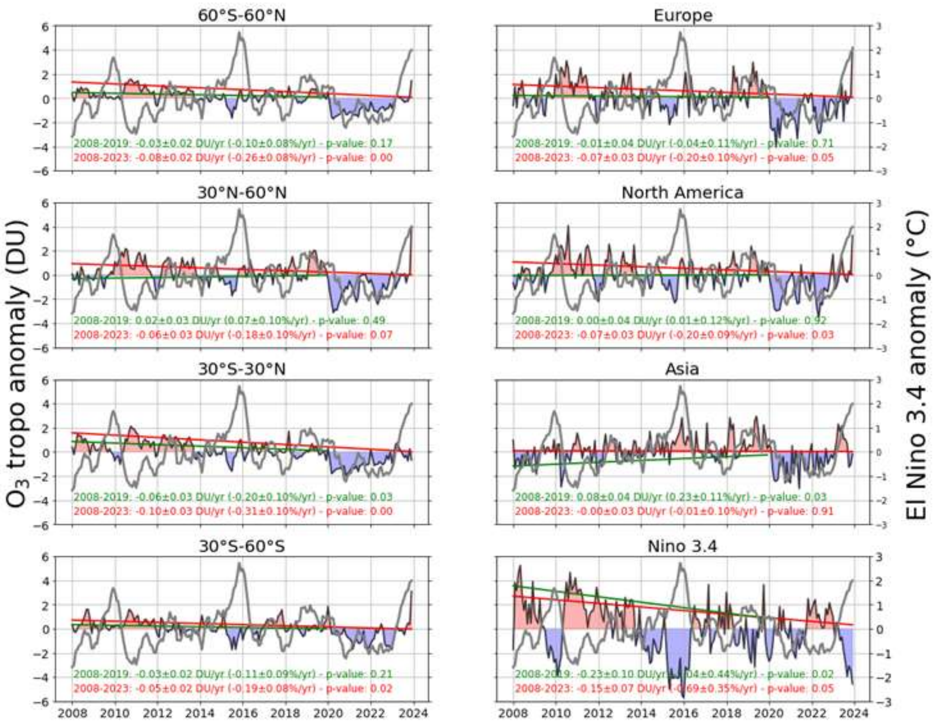

Figure 3. Monthly time series of TrO3 anomalies (in DU) derived from the L2 IASI TrO3 CDR product. The trend, uncertainty and p-value for the period before the COVID-19 pandemic (2008-2019) and including the pandemic (2008-2023) are indicated on each plot in green and red, respectively. Monthly El Nino 3.4 index values are plotted in grey. Figure from Boynard et al. (2025).

3.2 WP 2: Harmonisation of tropospheric ozone data records

Different satellite sensors and measurement techniques perceive the tropospheric ozone field differently. In fact, the community recognises that these differences are likely a prime contributor to the observed differences in global ozone burden, its spatial distribution and long-term trends (Gaudel et al., 2018). In order to improve consistency between the data records, the TAPIOWCA team developed and applied a harmonisation scheme to reduce the effect of the different tropospheric perspective for all satellite data sets contributing to major assessments.

3.2.1 Correcting and characterising differences in vertical representations

Methods

The main goal of this work package is to address some of the challenges in interpreting the spatial distribution and long-term evolution of satellite ozone data records identified in the first Tropospheric Ozone Assessment Report (Gaudel et al., 2018). While TOAR concluded to a reasonably good agreement of the tropospheric ozone burden between satellite data records at the near-global, multi-annual mean level, it proved more challenging to assess the ozone burden at the regional scale, and especially to determine the sign and magnitude of long-term changes. These challenges were believed to be at least partially due to inherent differences between the satellite data in terms of unit representation, vertical smoothing, a-priori information, uncertainty characterisation, and spatio-temporal sampling, including the definition of the tropospheric top level as a major contributor. Our primary methodological objective was therefore to harmonise the vertical perspective of different ozone data records from satellites, for the two main classes of products that currently exist, and using the Copernicus Atmosphere Monitoring Service Re-Analysis (CAMSRA) as a transfer standard. The first class of tropospheric ozone products is obtained from nadir-viewing sounders, where spectral irradiance observations are retrieved into Level-2 vertical ozone profiles. The second class of products consists of the subtraction of a stratospheric component from total column retrievals, which yields Level-3-type tropospheric ozone column data.

Appropriate choices of new prior profiles and prior constraints within the Complete Data Fusion framework allow nadir ozone profile harmonisation (which requires the availability of averaging kernel matrices) in several ways. In order to avoid the known difficulties of the maximum-likelihood and information-centred representations, only the a-priori profile replacement (APR) and unit-sensitivity representation (USR) methods were considered in this work, with only the former making use of retrieval re-constraining using CAMSRA. Also for the tropospheric residual column products, two top level harmonisation approaches were considered: while the column-averaged volume mixing ratio (XO3) method assumes a flat vertical ozone distribution throughout the free troposphere, the fill-in method does not, and instead uses the CAMSRA profile shape to correct for the different vertical extent of the tropospheric columns. Using these methods, all products from both classes can be harmonised to obtain a tropospheric ozone column with a common top level, and common prior information where applicable. Eventually, our harmonisation assessment focused on those methods that are (re)constrained by the CAMS reanalysis, i.e. APR for the profile products and the fill-in method for the column data.

Results

The first task of WP 2 resulted in the delivery of sixteen harmonised satellite tropospheric ozone data records (single net-CDF file) onto the BIRA-IASB data repository, see reference below. **Figure 4** shows the satellite datasets time series before (left) and after (right) harmonisation, providing a view of the reducing effect of the eventually chosen harmonisation operations on the inter-product dispersion.

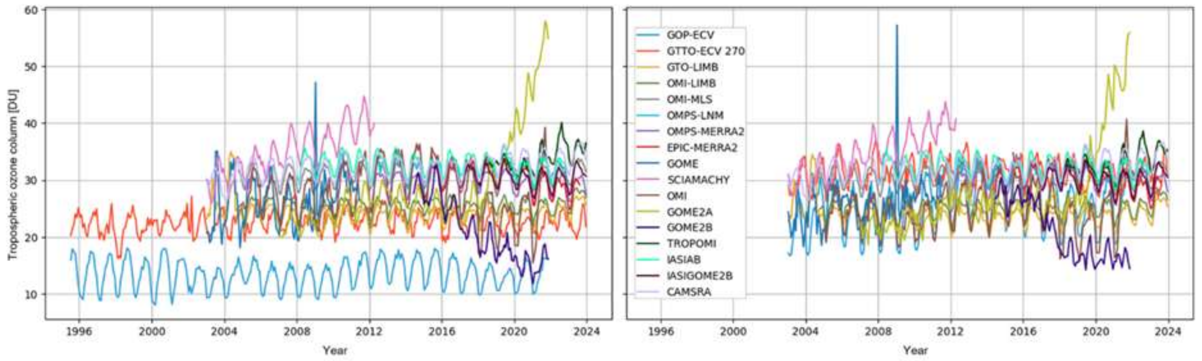

Figure 4. Near-global (60° N–60° S) tropospheric ozone column time series for all sixteen satellite data records and CAMSRA, both before (left) and after (right) harmonisation. Note that the latter is limited to the CAMSRA temporal domain (2003-2023). Figure from Keppens et al. (2025).

Reference: Keppens, A., Hubert, D., Granville, J., & Lambert, J.-C. (2025). Harmonised satellite tropospheric ozone Climate Data Records (TAPIOWCA) (Version 1) [Data set]. Royal Belgian Institute for Space Aeronomy. https://doi.org/10.18758/r7u4z0he

3.2.2 Characterisation of remaining measurement uncertainties

Methods

Our harmonisation objective has been translated into two major research questions, addressing (1) whether the mutual consistency of satellite data sets, both in terms of their mean distributions and long-term changes, is improved by data harmonisation, and (2) whether this harmonisation does not worsen the agreement of the satellite data with ground-based reference observations. We considered monthly mean ozonesonde data obtained from the TOAR-II HEGIFTOM working group for the latter, and compared with the Level-3 (harmonised) satellite data for grid cells that contain one of the 43 launch sites. Note, however, that in contrast with the performance assessment for the nadir ozone profile harmonisation, there is little use in comparing pre and post harmonisation anchoring for the column datasets, given that the top level for the vertical ozonesonde profile integration is always matched with the top level of the satellite product.

Results

Figure 5 summarises the dispersion on the difference between monthly time series of satellite and Level-3-like ozonesonde tropospheric columns for four nadir profile products (OMI, TROPOMI, IASI-AB, and IASI+GOME-2B) and for two tropospheric top level definitions (fixed 450 hPa pressure and the lapse-rate tropopause). For each data point, the satellite data time series is limited to the single grid cell covering the respective ground station (43 in total, sorted north to south). The dispersions on the satellite-ground difference time series have been calculated for the satellite weighted averages (WAV) and both harmonised profile products, APR and USR. The USR harmonisation effectively works for the lower-resolution (both horizontal and vertical) UV-visible retrieval products with an order of 10 % difference dispersion reduction, while it does not for the other products. The APR method slightly benefits (by about the same percentage) the higher-resolution TROPOMI and (combined) IR retrievals yet performs poorly for OMI. The dispersion however again shows a remarkable meridian dependence, with smaller values and harmonisation effects in the Southern Hemisphere, except for the USR applied to IASI-AB (Sepang airport, San Cristobal and Nairobi are roughly at the Equator).

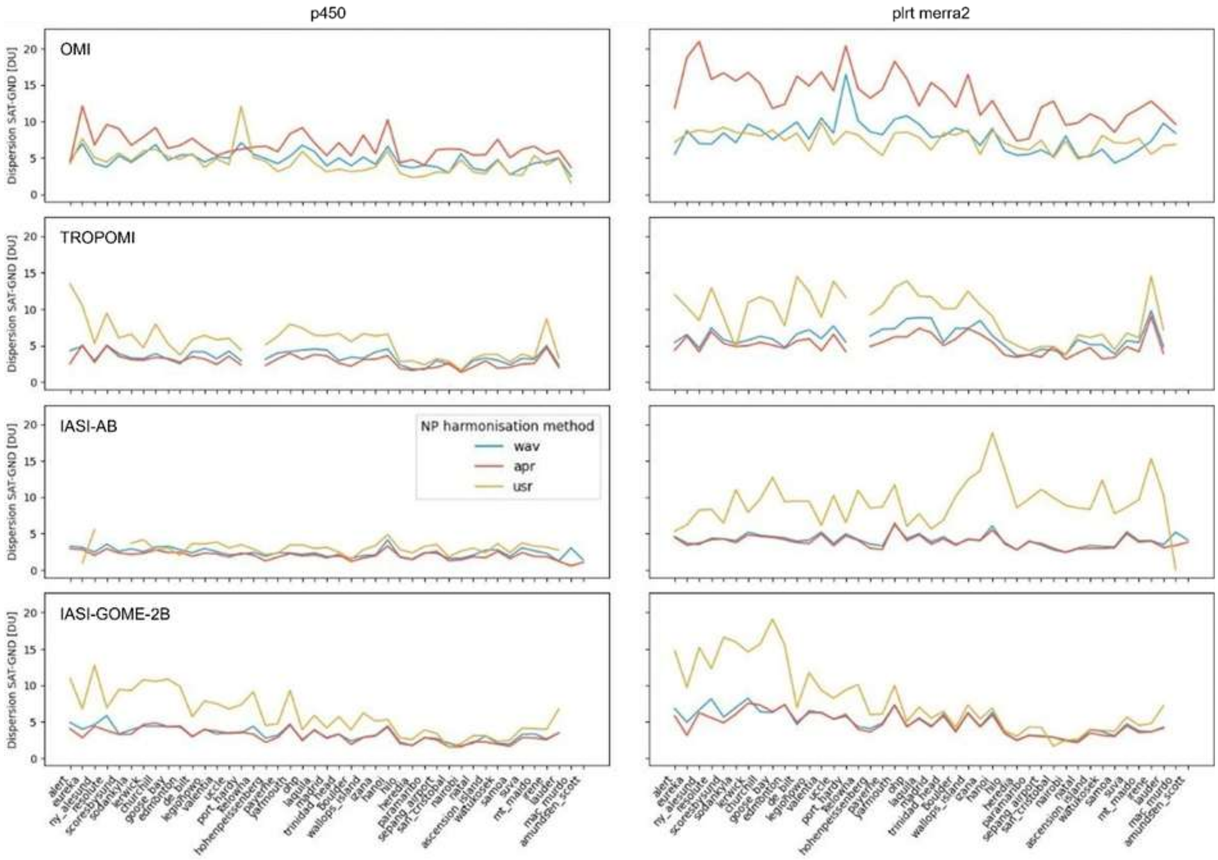

Figure 5. Dispersion on the difference between monthly time series of satellite (SAT) and Level-3-like ozonesonde (GND) tropospheric columns for four nadir profile products (OMI, TROPOMI, IASI-AB, and IASI+GOME-2B in rows, respectively) and for two tropospheric top level definitions (columns, 450 hPa fixed pressure level left and lapse-rate tropopause right). For each data point, the satellite data time series has been limited to the grid cell containing the respective ground station (sorted Arctic to Antarctic in each plot). Figure from Keppens et al. (2025).

Figure 6 shows that the largest reduction (about 2-4 DU) in inter-product dispersion (IPD) upon harmonisation is obtained for the residual column products (top, middle). Also the IPD of the spatial anomalies decreases (bottom, middle), though slightly (at most 1 DU), implying that harmonisation allows only slightly better constraints of small-scale spatial structure. The picture looks quite different for the APR harmonisation of the nadir profile products; their IPD reduction is mostly limited to parts of the Southern Hemisphere, with little differences between multi-annual columns or their spatial anomalies (left). It is interesting to note that for the three RAL products involved (OMI, GOME-2A, GOME-2B), lower tropospheric ozone column values are found in the northern mid-latitudes after harmonisation. Therefore, although their IPD is overall reduced by about 20 % upon APR, the latter also introduces a Northern Hemisphere bias with respect to the other three profile products here. When considering only the TROPOMI, IASI-AB, and IASI+GOME-2B datasets, the inter-product dispersion is reduced by 13 % upon APR harmonisation. Looking at all fourteen satellite products combined (right), the multi-annual mean IPD reduction upon harmonisation of the Level-3 column products prevails on the global scale (up to 40 %). For the anomalies (bottom), however, IPD increases between the profile products mostly outweigh the IPD reductions between the column products upon harmonisation, especially in the Northern Hemisphere.

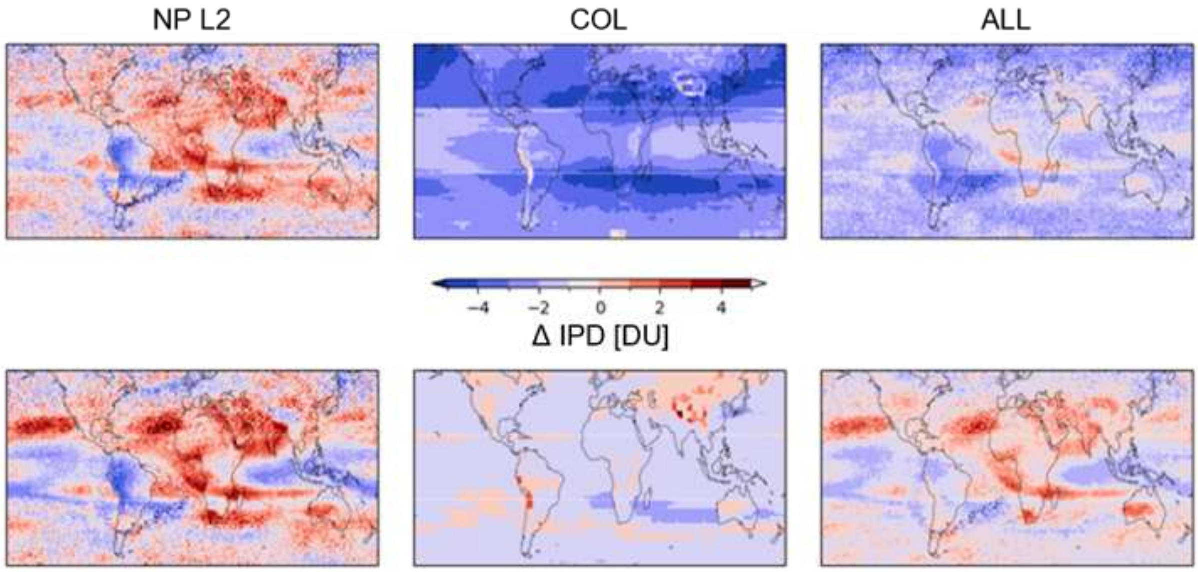

Figure 6. Change of the dispersion (IPD, in DU) between satellite data sets upon harmonisation (after minus before), for the 2018–2022 mean of fourteen satellite data products. The top row shows the absolute tropospheric ozone column values, the bottom row their spatial anomaly (i.e. after subtraction of the 60° S–60° N mean). The left and middle columns differentiate the results for all fourteen datasets (on the right) between the Level-2 profile products and the Level-3 column products, respectively. Figure from Keppens et al. (2025).

Looking at the profile and residual column products combined, the column fill-in method correcting for different tropospheric top level definitions appears to bring the highest gain in terms of IPD reduction (up to 40 %). This gain, however, mostly disappears when looking at the IPD of the anomaly time series of the column products only, which suggests that the fill-in harmonisation using a reanalysis rather mimics a global-scale inter-product bias correction. One could therefore also opt to apply this method to the lowest subcolumn of (vertically coarse) nadir ozone profile retrievals, as done for the Level-3 GOP-ECV product in this work by its lack of averaging kernels. For products with broad averaging kernels (effective vertical retrieval extents covering many layers), the latter might even be the preferred option, as it minimises the intrusion of stratospheric retrieval information into the tropospheric ozone column assessment. This approach is therefore also adopted in the TOAR-II satellite data assessment. The selection of the transfer standard for column fill-in harmonisation is however of importance as well, taking into account that the choice between a reanalysis or a climatology results in (spatio-)temporal differences in the correction term that can reach up to 2 DU or 5-10 % of the tropospheric ozone column.

3.3 WP 3: Improved attribution of observed ozone and water vapour changes

Multivariate regression techniques are widely used to disentangle the different geophysical processes responsible for observed variability and to quantify long-term changes. Both the optimal selection of terms in the statistical regression model, representing the expected mix of underlying processes and how these processes are best represented mathematically continue to be focal points of research. Ozone precursors and exchanges between stratosphere and troposphere are expected to influence long-term changes in tropospheric ozone abundances (e.g., Zeng et al., 2022), but these are rarely considered in trend assessments (Wespes et al., 2017). We therefore attempt to estimate the contribution of both processes by extending the regression model with additional terms (Tasks 3.1 and 3.2). Another target is to optimise the time lag between observed changes of ozone and the responsible atmospheric process (Task 3.3). The latter has not yet been fully explored in trend studies

3.3.1 Attribution of tropospheric ozone trends to CO as an ozone precursor

The goal of this task is to investigate whether changes in ozone precursor concentrations, in particular CO, can explain, at least, part of the trend in IASI merged TrO3 (see WP 1, Section 3.1.1) using multiple linear regression (MLR) techniques.

Ozone precursors are expected to influence long-term changes in TrO3 abundances but these are rarely considered in trend assessments (Wespes et al., 2017). To that end, we exploit here the ability of IASI to simultaneously measure O3 and CO in the troposphere. The O3-CO relationship is first examined to apprehend the influence of continental pollution on O3 trends observed by IASI in the troposphere. A IASI CO proxy is then developed and added in the MLR model to account for such a relationship.

Methods

We use an MLR approach to disentangle the different geophysical processes responsible for observed variability in O3 levels and to better quantify anthropogenic long-term changes in the troposphere. A reference MLR model that includes a series of proxies used to account for a linear trend, for variations related to dynamical processes (QBO, North Atlantic Oscillation - NAO, Antarctic Oscillation - AAO, ENSO), for the solar flux and for the volcanic aerosols is used to adjust the daily merged IASI TrO3 columns provided in WP 1 (see Section 3.1.1). In order to account for the role of CO, as O3 precursor, in TrO3 changes, one additional proxy built from IASI total CO measurements (IASI L2 ULB-LATMOS CDR dataset based on the FORLI-CO v2015 retrieval algorithm) is added to the MLR model, which constitutes the target MLR model. The CO proxy is a 1°x1° gridded daily time series normalised over the period of IASI observations. The MLR is performed using an iterative stepwise backward elimination approach that aims to retain the most relevant proxies at the end of the iterative procedure. Their associated standard errors are estimated from the covariance matrix of the regression coefficients.

Results

The analysis of the O3-CO relationship detected by IASI is first examined in terms of correlation coefficient, regression slope and covariance (**Figure 7**) for a better understanding the origin of O3 trends in the troposphere. Indeed, it allows to differentiate tropospheric and stratospheric air masses and to identify the regions influenced by continental export/intercontinental transport of ozone pollution (e.g., due to biomass burning and lightning).

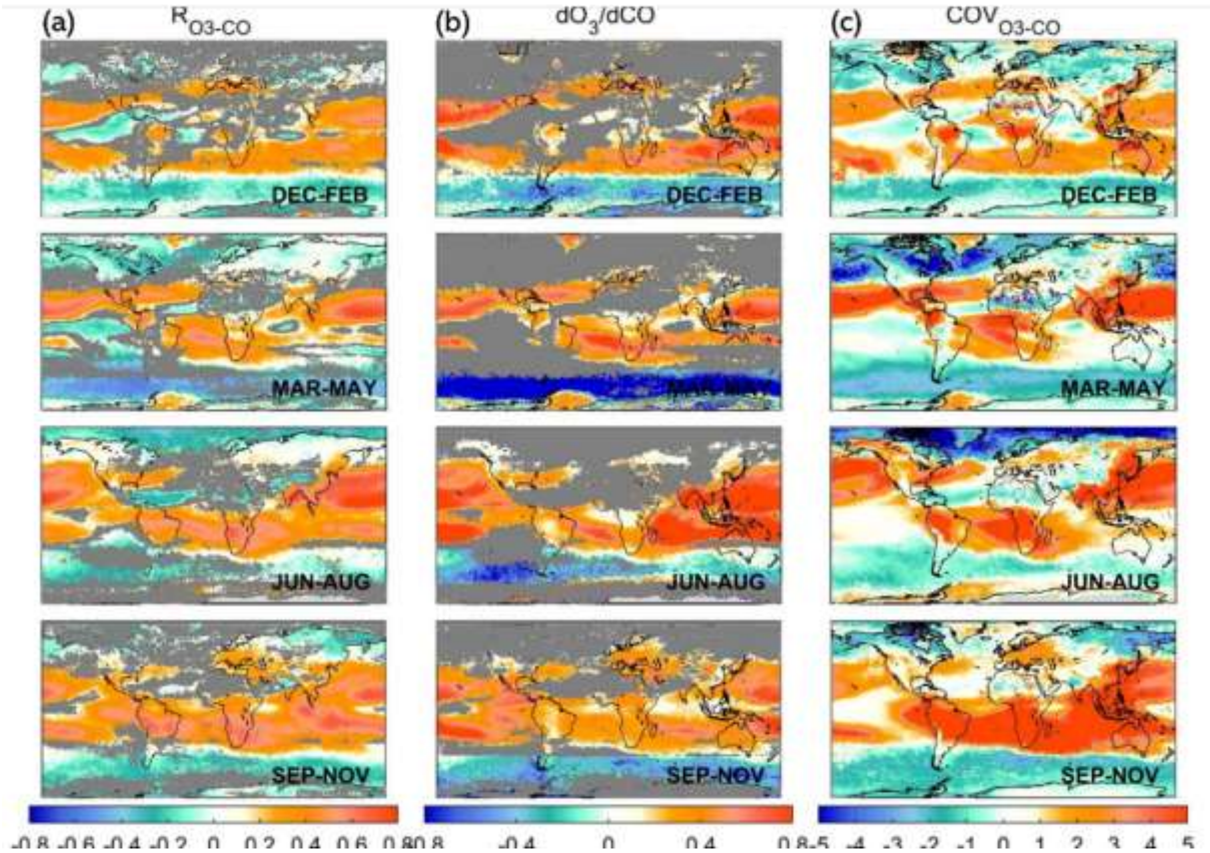

Figure 7. Seasonal distributions of (a) the correlation coefficients (R_{O3-CO}), (b) the regression slope (dO3/dCO in mol.cm^{-2} / mol.cm^{-2}) and (c) the covariances (COV_{O3-CO} in 10^{33} mol.cm^{-2} × mol.cm^{-2}) of daily merged IASI TrO3 and daily merged total CO over 2008-2023. Data are averaged over a 1°x1° grid cells. Crosses in R_{O3-CO} and dO3/dCO panels are non-significant grid cells (2σ level).

The O3-CO correlation patterns allow to distinguish outflow regions characterised by photochemical O3 production from precursors, here CO, or by CO destruction (positive correlations) from regions characterised by O3 loss or by strong stratospheric contaminations (negative correlations). The O3-CO enhancement ratio dO3/dCO is used to evaluate the photochemical O3 production in continental outflow regions from CO, while the covariance helps to identify the regions with the highest pollution variability. Maxima in R_{O3-CO} and dO3/dCO are detected in continental pollution outflow regions during the peak of photochemistry in summer in the NH, especially downwind South-East Asia, and, also over the South Africa/Amazonia/South Atlantic regions during the dry season, originating, respectively, from Asian pollution influence and from combustion sources including biomass burning. The strong positive O3-CO relationship in terms of R_{O3-CO}, dO3/dCO and COV_{O3-CO} measured over and downwind of East India/China in summer in comparison with the ones measured downwind of East US and over Europe indicate that South-East Asia experiences the most intense pollution episodes in the NH over the IASI period. The results clearly demonstrate the role of CO on TrO3 levels captured by IASI.

In order to further evaluate the continental influence on TrO3 changes, both reference (without CO proxy, **Figure 8** bottom left) and target (with CO proxy, **Figure 8** bottom right) runs were applied to IASI merged TrO3 columns. **Figure 8** also shows the IASI TrO3 response to CO (top).

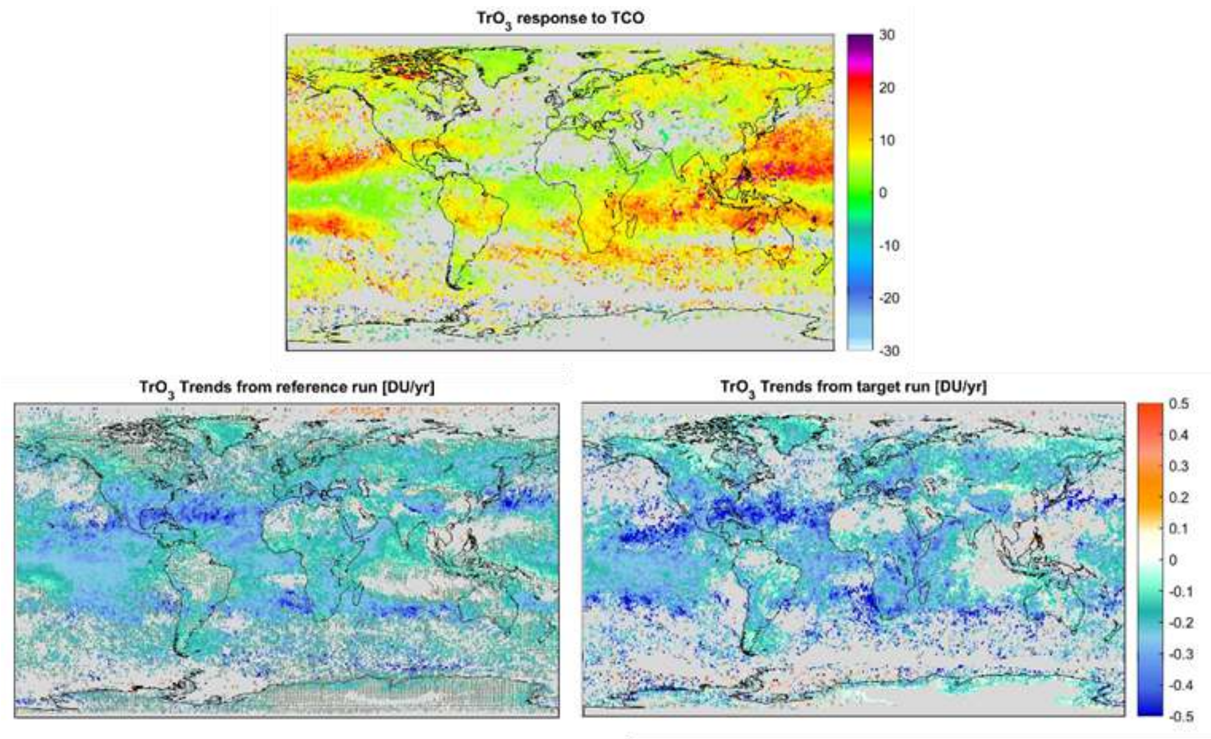

Figure 8. Global distribution (a) of annual regression coefficient estimates (DU) for CO proxy in IASI merged TrO3 target MLR adjustment, (b and c) of trends (DU per year) in IASI merged TrO3 derived from reference MLR adjustment (without IASI CO proxy) and from target MLR adjustment (with IASI CO proxy), respectively. The grey areas and crosses represent non-significant grid cells (2σ level).

We found that

1. the adjusted CO coefficients inferred from the target run show very similar patterns to those of O3-CO relationship discussed above (**Figure 8**), indicating that the role of CO as TrO3 precursor and as driver of its variability is clearly identified by MLR.
2. the adjusted CO coefficients estimate in the target run are all positive, indicating only an in-phase relation between CO and O3 (i.e. an increase in CO drives an increase in TrO3, or vice versa). The large amplitude of CO signal show that CO largely contributes to TrO3 levels and variability.
3. the trend is more likely to be rejected by the stepwise-fit iterative procedure in case of target MLR (see grey areas in **Figure 8**), indicating that the inclusion of the CO proxy reduces the significance of the fitted trend in the MLR. This is, in particular, observed above South-East Asia/Indonesia where the O3-CO relationship is the highest (**Figure 7**). This tends to indicate that CO compensates/explains, to some extent, the TrO3 trends.

Nevertheless, large negative trend estimates inferred from the target MLR remain or are amplified, in particular, in the eastern US over the Atlantic. In order to understand this effect, lagged TrO3 response to CO could be investigated by including lagged CO proxy in the target MLR. The use of a seasonal MLR model could also help. It should also be noted that the significant large negative trend become insignificant or not retained by the iterative procedure when the target MLR is applied to 2008-2019 data before the COVID lockdown period (not shown here).

3.3.2 Attribution to Stratosphere-Troposphere Exchange

The objective of this task is to investigate whether stratosphere-troposphere exchanges (STE), which inject ozone-rich stratospheric air into the troposphere, influence long-term changes in tropospheric ozone abundances, using an MLR approach with dedicated proxies to account for STE processes.

Indeed, at mid-latitudes, STE often occur during tropopause fold events. Such tropopause folds occur more frequently than before due to increased stratospheric wave activity and an accelerated Brewer Dobson circulation, which, in turn, is expected to lead to increasing abundances of ozone in the troposphere (Akritidis et al., 2019; Abalos et al., 2021; Bartusek et al.,2023). Although tropopause folding is a dynamically reversible process, the associated transport of stratospheric air into the troposphere is largely irreversible. This underlines the interest in studying the influence of STE on TrO3 using MLR techniques.

Methods

As in Section 3.3.1, an MLR approach is used to disentangle anthropogenic long-term changes in the troposphere from the different geophysical processes responsible for observed variability in TrO3. In addition to the proxies used in the reference model, geopotential height (GEO) and potential vorticity (PV) proxies taken from the ERA-5 reanalysis are added to the MLR to infer the contribution of STE to observed long-term changes in TrO3. This constitutes the target run. The GEO and PV proxies are 1°x1° gridded daily time series of GEO and PV at 250 hPa normalised over the IASI period. They account, respectively, for changes in the tropopause height and in the mixing of tropospheric and stratospheric air masses (Wespes et al., 2017), which characterised well STE processes at mid-latitudes.

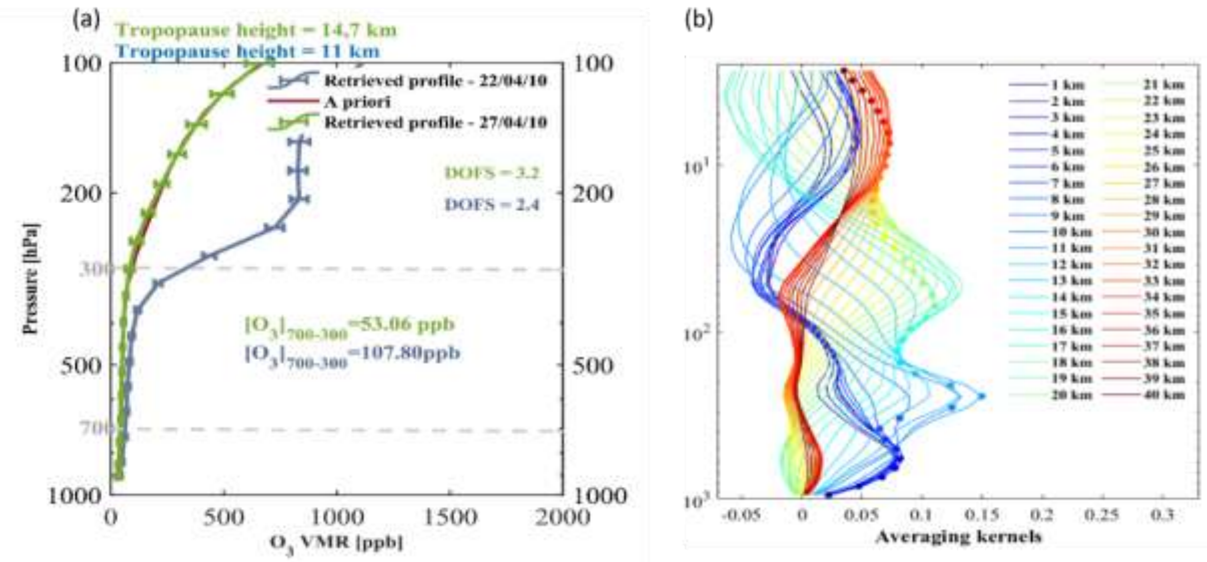

Figure 9. (a) Typical example of FORLI-O3 retrieved profile (ppb) from the surface to 100 hPa associated with a STE event (22 April 2010, in blue). The O3 profile a few days after this STE event is shown for comparison (27 April 2010, in green). (b) Corresponding averaging kernel functions.

Results

Before performing an MLR analysis, the ability of IASI to detect STE events in TrO3 columns is first examined. To that end, numerous cases of STE events were flagged in IASI data based on ERA-5 GEO and PV values, on IASI thermal tropopause height and on their anomalies. These cases are all characterised by a strong ozone increase in the upper troposphere / lower stratosphere (UTLS) down to about 300 hPa (**Figure 9** for an STE event on 22 April 2010). Such events also have increased IASI sensitivity to ozone in these layers, leading to increased total degrees of freedom for signal.

A local increase in TrO3 levels during STE is further illustrated in **Figure 10** (see pink circle) which shows the global distribution of (a) IASI TrO3 (from ground to 300 hPa, in order to identify the STE increase in O3 below the tropopause), (b) tropopause height, (c) geopotential height and (d) potential vorticity (both at 300 hPa, taken from ERA-5).

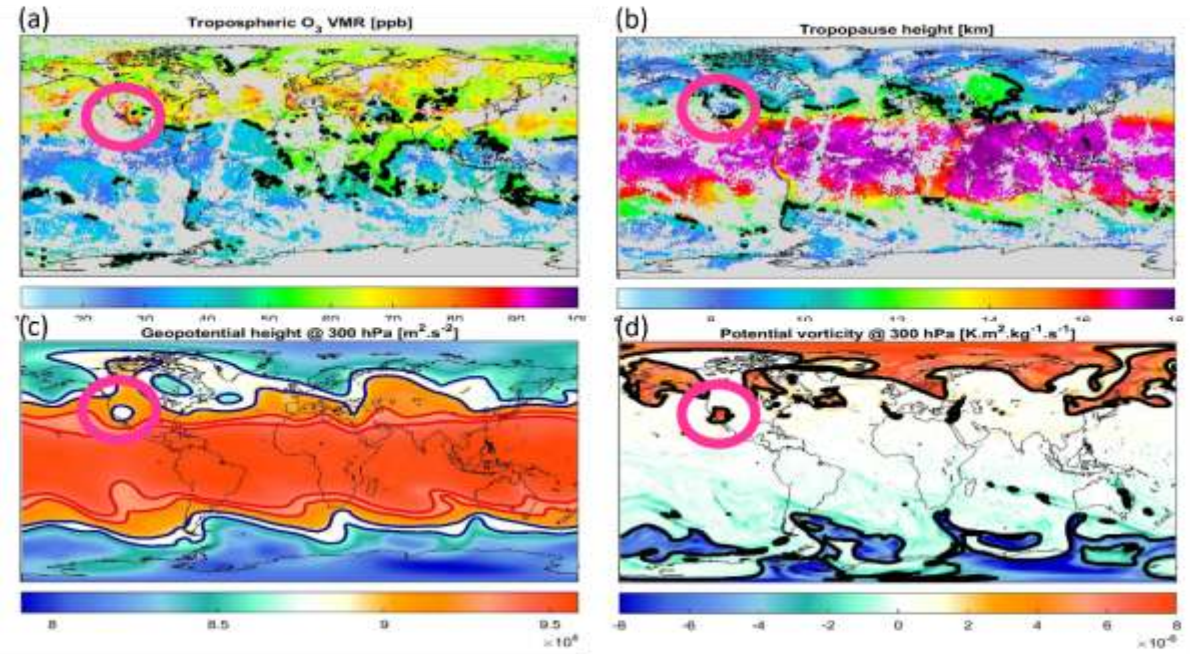

Figure 10. Global distribution on 22 April 2010 of (a) IASI ozone (ground to 300 hPa; ppb), (b) tropopause height, (c) geopotential height (at 300 hPa) and (d) potential vorticity (at 300 hPa) corresponding to a detected STE event over California, US (see pink circle). Isocontours delimit the polar (blue) and subtropical (red) jet streams.

After demonstrating that IASI is sensitive to STE-induced TrO3 variations, the target MLR run, which includes the GEO and PV proxies, was applied to TrO3 data to estimate how the two proxies drive its variation. **Figure 11** illustrates the IASI TrO3 response to both GEO and PV (top panels), as well as TrO3 trends inferred from the reference and the target runs (bottom panels) over the IASI period.

We found that

1. the adjusted GEO and PV coefficients inferred from the target run show specific patterns with a large amplitude of their signal. In particular, the band-like pattern of negative GEO coefficients found at mid-latitudes (mainly in the NH) coincides with the STE detections around and between the subtropical and the polar jets (not shown here). That out-of-phase TrO3

variations likely indicates an increase in TrO3 columns when the geopotential height decreases, while fitted PV coefficients in that band show opposite behaviour with an in-phase TrO3 variations, i.e. an increase in PV drives an increase in TrO3. This specifically occurs in case of STE events at these latitudes (**Figure 10**). These results tend to indicate a significant role of both GEO and PV as driver of TrO3 variability in mid-latitudes. Other band-like patterns in GEO and PV coefficient distributions require further examination.

2. The inclusion of the two proxies in the MLR model increases the robustness of the fitted negative trends, especially at extratropical latitudes where insignificant trends in the reference MLR become significant in the target MLR (see **Figure 11**, panels c and d). It likely indicates that increases in TrO3 levels due to STE events affect the trend adjustment in MLR which highlights the significant role of STE on estimated TrO3 changes.

Nevertheless, at this stage, likely compensation effects between adjusted proxies and trends in TrO3 are suspected and still require further investigation. For instance, the use of only one of the two target proxies could be investigated.

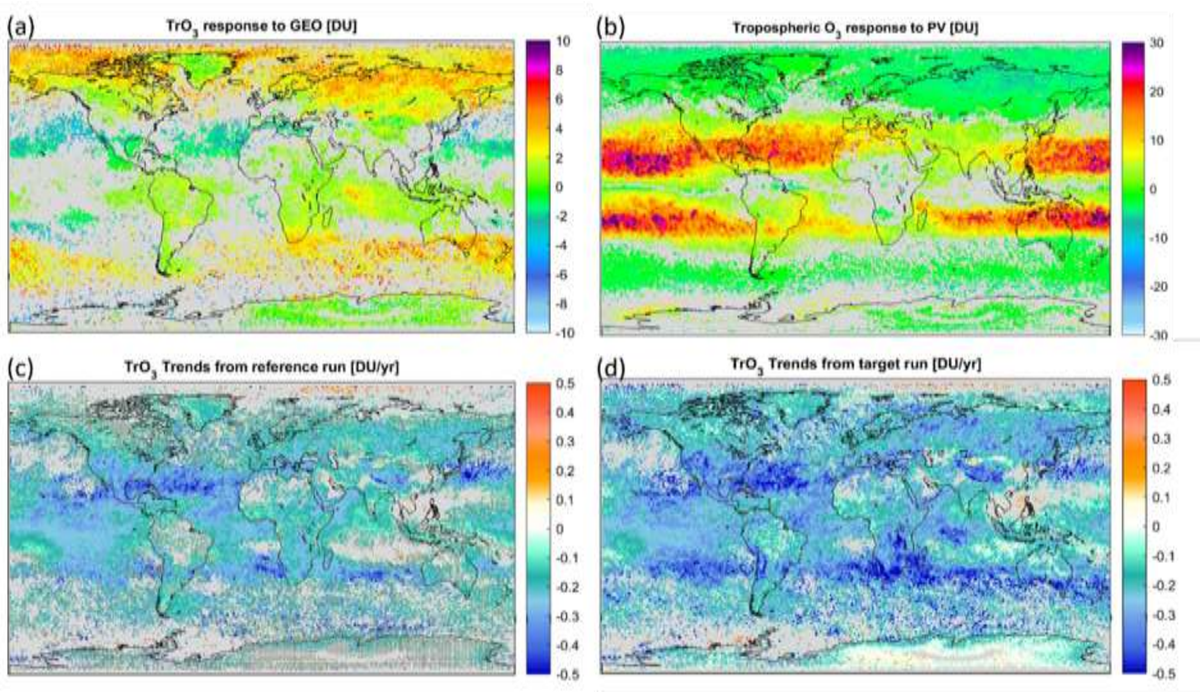

Figure 11. Global distribution of annual regression coefficient estimates (top; DU) for the GEO and PV proxies (a, b) in IASI merged TrO3 target MLR adjustment and trends (bottom; DU per year) in IASI merged TrO3 derived from reference MLR adjustment (c, without GEO/PV proxies) and from target MLR adjustment (d, with GEO/PV proxies). Greyed areas and crosses represent non-significant grid cells (2σ level).

3.3.3 Optimisation of proxy time lag

The El Niño Southern Oscillation (ENSO) modulates atmospheric trace gas concentrations at time scales of 2-7 years (Domeisen et al., 2019). ENSO variability is widely accounted for in stratospheric ozone time series analyses to avoid biased estimates of long-term trends and to strengthen constraints. However, most trend studies assume, without much quantified motivation, an instantaneous response of stratospheric ozone concentrations to ENSO events at Earth's surface (WMO, 2022). We therefore investigated the possibly lagged response of stratospheric ozone to ENSO more closely and verified whether the inclusion of an ENSO lag in the time series analysis helps improve the robustness of long-term ozone trend assessments.

Methods

We developed a cross-correlation method to estimate the response time of ozone to ENSO at each vertical level and latitude. Since the impact of ENSO on ozone concentrations is generally weaker than other processes (e.g., QBO, solar cycle, aerosol load), the latter were first removed from the observations. The resulting ozone residuals were then cross-correlated with a lagged ENSO predictor time series over the period 2000-2024, since measurement uncertainty is considerably better than during 1984-1999. Next, we searched for the time lag corresponding to the peak value in the correlograms, and estimated its uncertainty (**Figure 12**). This method was applied to three widely used merged satellite data records: SAGE-CCI-OMPS+ (Sofieva et al., 2023), SWOOSH (Davis et al., 2016), and GOZCARDS (Froidevaux et al., 2015) which provide monthly zonal mean ozone profile observations between October 1984 and December 2024.

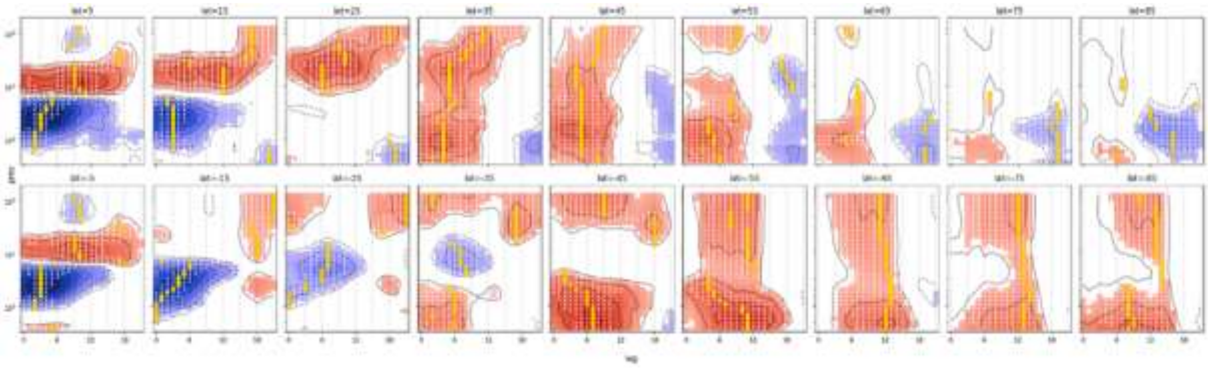

Figure 12. ENSO-ozone correlograms (x-axis: time lag, months; y-axis: pressure, hPa) across the stratosphere (left to right: EQ-10° latitude, 10°-20°, …, 80°-90°; top: Northern Hemisphere, bottom: Southern Hemisphere) for the SAGE-CCI-OMPS+ data record. The colour scale shows correlation (red: positive, blue: negative). Yellow markers indicate peak lag and white markers its corresponding 68% confidence interval.

Results

Figure 12 shows the correlograms for SAGE-CCI-OMPS+, but results are similar for GOZCARDS and SWOOSH. The observed patterns agree with expectations. Negative correlations in the tropical lower stratosphere are due to faster upwelling during the El Niño phase (or slower during the La Niña phase), which pushes ozone-poor tropospheric air into the ozone-rich lower stratosphere. The correlation changes sign around 10-20 hPa because of a change in sign of the vertical gradient of the ozone field. In the tropics, lag estimates increase with altitude: from 1-3 months (lower stratosphere), to 6-9 months (middle stratosphere) and up to 12-18 months (upper stratosphere). Elsewhere, correlograms and peak lags carry the imprints of the large scale Brewer Dobson circulation. At mid-latitudes, lag values of 4-10 months follow the (descending) shallow branch below 50 hPa or the (ascending) deep branch above 5-10 hPa. The deep branch descends into the polar regions, leading to lags of up to 12-15 months.

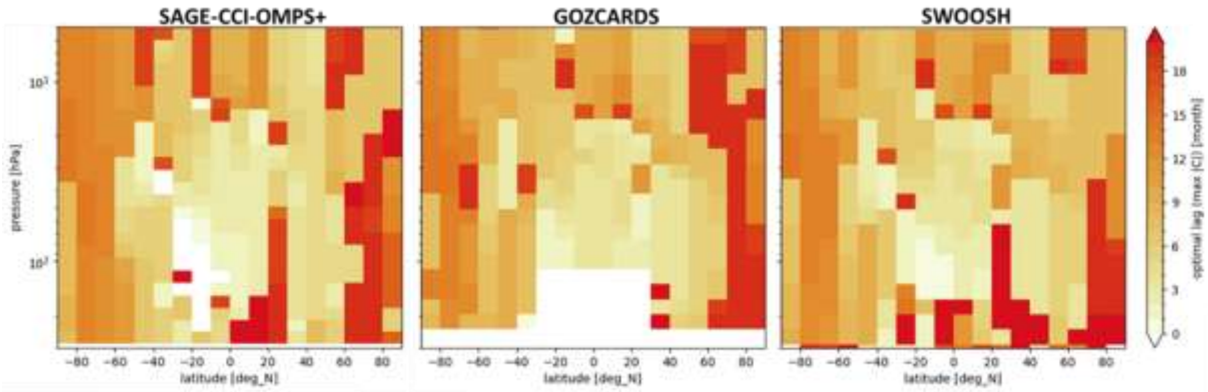

Figure 13. Spatial structure of ENSO time lag estimates (in months) for three merged records (left to right).

Figure 13 shows an overall consistent structure of peak lag across the stratosphere for the three satellite data records. Several regions (e.g., Arctic and low/mid-latitude lower stratosphere) have noisy or flat correlograms that render the identification of their peak value difficult. Further work will be required to improve the spatial stability of lag estimates, and to combine the results of the three satellite records in one best estimate of the ENSO lag field.

3.4 WP 4: Assessment of present and past changes in ozone and water vapour distributions

3.4.1 Assessment of tropospheric ozone

The first Tropospheric Ozone Assessment Report (TOAR) found important differences between satellite tropospheric ozone records (Gaudel et al., 2018). The sign of global ozone burden trends (mid-2000s to mid-2010s) was not reconcilable and mean tropospheric ozone values during 2010-2014 differed at smaller (regional) scales. Also, the annual cycle could not be investigated at monthly resolution, but at seasonal resolution.

The second phase of TOAR (TOAR-II) was able to address these issues by using more satellite records with improved data quality, longer time series, higher spatial resolution, and a common definition of the tropospheric ozone column (surface to thermal tropopause, see Section 3.2.1). The TOAR-II assessment of satellite observations (Hubert et al., 2026), led by the TAPIOWCA coordinator, assesses the mean state and the seasonal cycle of tropospheric ozone during 2018-2022, estimates long-term changes since the mid-2000s, and focuses on special events such as the COVID-19 pandemic and extreme wildfires.

Methods

Fifteen harmonised satellite records were extensively intercompared, then combined to estimate multi-annual mean ozone, seasonal cycles, and long-term changes. The combination method was designed to reduce sensitivity to outliers, limit the influence of biases between datasets, use ensemble spread to characterise uncertainty, and provide conservative uncertainty estimates.

Long-term ozone trends were estimated using multiple linear regression, including a single linear trend term, predictors for ENSO and QBO variability, and treatment of autocorrelated residuals. Since the combined satellite ozone time series show clear long-term non-linearity, the trend estimates change with the start and end time.

Results

The overall agreement between the harmonised satellite records is considerably better than the data available for TOAR-I, which resulted in smaller uncertainties and more finely resolved results in the spatial domain and in the annual cycle. Further improvements in calibration, retrieval and harmonisation schemes will be key to improving future assessments, most notably to reduce the impact of prior differences on the mean distribution, to increase data quality at higher latitudes and to improve the agreement between ozone time series from the residual measurement technique and from the UV-visible or infrared nadir profiling techniques.

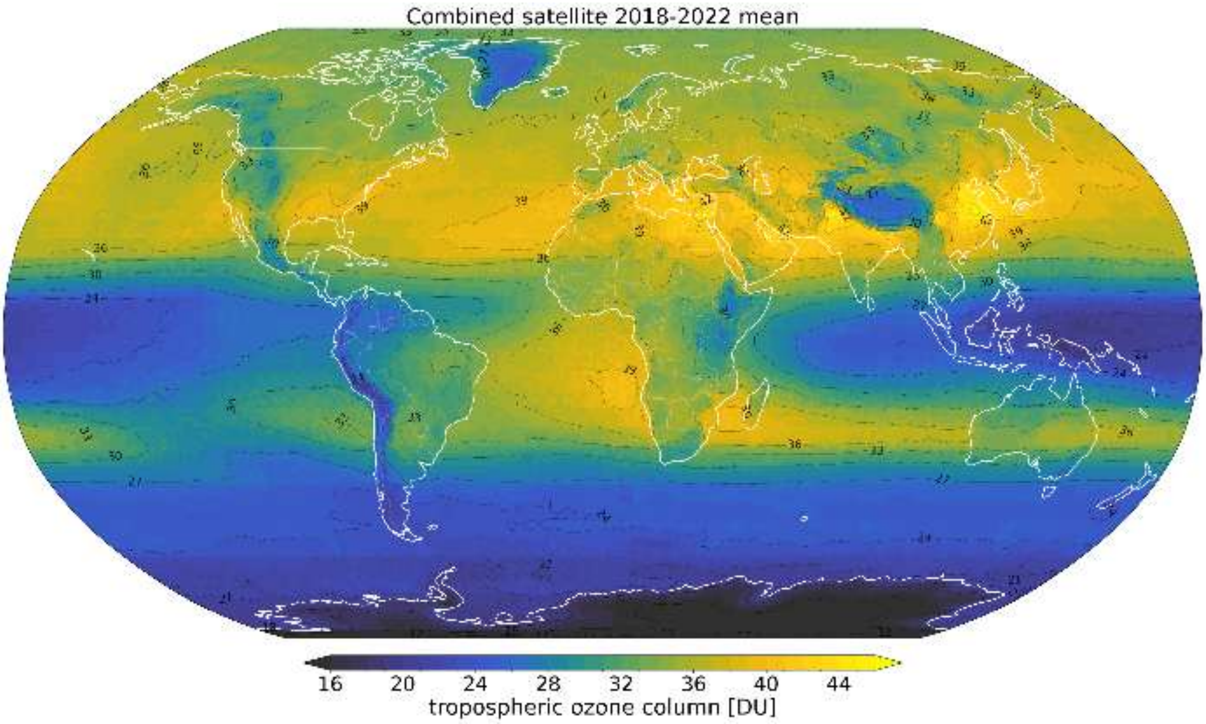

Figure 14. Distribution of tropospheric ozone (DU) during 2018-2022 inferred from a combined satellite record. Figure from Hubert et al. (2026).

Figure 14 shows the mean tropospheric ozone column during 2018-2022 at 1° spatial resolution, with highest values over polluted and downwind Northern Hemisphere regions, especially central-eastern China (global maximum of 46 DU), and lowest values over Antarctica (global minimum of 10 DU) and remote Southern/tropical oceans. The observed patterns reflect multiple processes, including photochemical production in regions with, or downwind of, strong precursor emissions and favourable meteorological conditions; intercontinental and convective transport; stratosphere-troposphere exchange; and variations in tropospheric depth driven by orography and tropopause altitude. The global tropospheric ozone burden during 2018-2022 is 336 ± 6 Tg, closely matching the TOAR-I value of 339 ± 8 Tg for the 2010-2014 period but with a more reliable and a better constraint due to more records and improved uncertainty treatment.

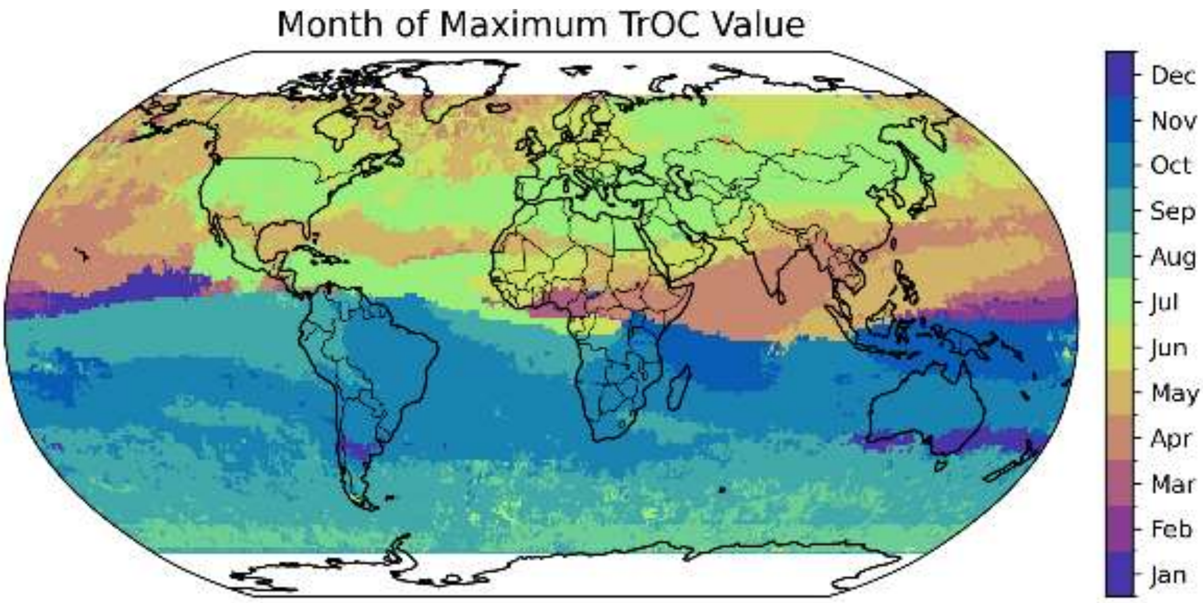

Figure 15. Month with largest tropospheric ozone column in the 2018-2022 mean annual cycle. Figure from Hubert et al. (2026).

The combined satellite estimate reveals a strong seasonal cycle in both hemispheres, with maxima mainly in July across the Northern Hemisphere mid-latitudes from North America to East Asia (**Figure 15**). Seasonal amplitudes are largest in this band, reaching 15-30 DU, with broad summer maxima over the United States, Europe, China, and the Middle East. These patterns likely reflect anthropogenic precursor emissions, stratosphere-troposphere exchange, and regional transport. The timing of the maximum shifts earlier toward tropical Northern Hemisphere regions, possibly linked to the Asian Summer Monsoon and associated transport of cleaner marine air.

The combined product resolves regional structures not available in TOAR-I. From Europe to East Asia, ozone rises in spring over the North China Plain and Indo-Gangetic Plain, reaching up to 60~DU, then extends westward into Central Asia, the Middle East, and the Eastern Mediterranean in summer. Over the North Atlantic, enhanced ozone develops from the eastern United States and is transported eastward, forming a 45-50 DU ozone belt. In the Southern Hemisphere, TrOC peaks in September-October over the South Atlantic, southern Africa, and Amazonia, likely influenced by lightning NOx, biomass burning, and stratospheric transport.

Figure 16 shows 5° global maps of tropospheric ozone trends since January 2005, estimated from the combined satellite record and evaluated for two end dates: December 2019 (top) and December 2022 (bottom). The comparison reveals a marked shift in trend after 2019. From 2005 to 2019, near-global mean (60°S – 60°N) tropospheric ozone increased by +1.0 ± 0.4 % per decade (high confidence), with the strongest positive trends (+2-4 % per decade, very high confidence) extending from Central Siberia to South Asia and the extratropical North Pacific. Additional increases occurred from the Middle East to the Caribbean, over northern Europe, western Canada, Brazil, and the extratropical South Pacific. High-confidence decreases were limited mainly to the central equatorial and eastern South Pacific (-2-3 % per decade), while negative Arctic-region trends had low confidence. Extending the record to 2022 reverses the near-global mean trend to -0.6 ± 0.5 % per decade (low confidence), due to a sustained decline during 2020-2022.

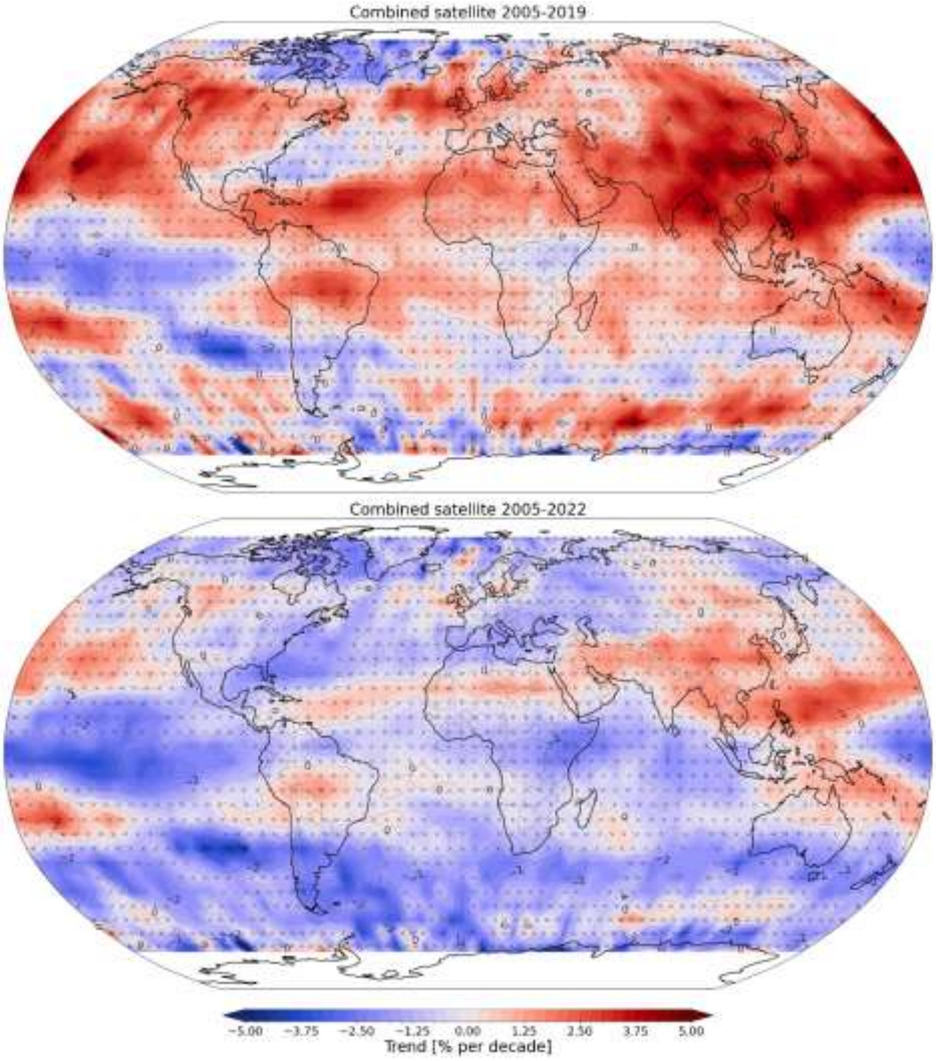

Figure 16. Tropospheric ozone trend (% per decade) between January 2005 and December 2019 (top) or January 2005 and December 2022 (bottom) inferred from a combined satellite record. Results with very low to medium confidence are stippled. Figure from Hubert et al. (2026).

3.4.2 Assessment of stratospheric ozone

Ozone trends in the lower stratosphere remain uncertain due to the combined effect of larger natural variability and measurement uncertainty when compared to higher up in the stratosphere (WMO, 2022). ENSO is a phenomenon at Earth's surface and an important driver of interannual variability of stratosphere ozone concentrations, especially in the lower stratosphere. While the community baseline regression model includes an ENSO term, it does not account for a lagged response. Here, we use the results from WP 3 (Section 3.3.3) and study the impact of including lag, or not, on 2000-2024 trend estimates and their uncertainty for three satellite records (SAGE-CCI-OMPS+, SWOOSH and GOZCARDS).

Methods

We derive trends through a multiple linear regression (MLR) of deseasonalised ozone anomalies to the baseline statistical model used by the APARC LOTUS community (SPARC/IO3C/GAW, 2019; Godin-Beekmann et al., 2022; Sofieva et al., 2025) and the last few WMO Ozone Assessments (WMO, 2018, 2022). It consists of regressor terms for ENSO, QBO, solar cycle, and aerosol load. The trend term consists of two independent linear trends, the first ending in 1997, the second starting in 2000

$$Y(t) = \gamma_1\ QBO_1(t) + \gamma_2\ QBO_2(t) + \gamma_3\ SOLAR(t) + \gamma_4\ AEROSOL(t) + \gamma_5\ ENSO(t + \tau) + TREND(t) + Noise$$

We applied this method to the three merged satellite data records also considered in Section 3.3.3. The MLR is run in three configurations: without ENSO term, with an unlagged ENSO term (τ=0), and with a lagged ENSO term ($\tau > 0$) using lag estimates for each data set (**Figure 13**).

Results

2000-2024 trend estimates differ by 0.1-0.5 % per decade if the ENSO term is lagged, with respect to trends estimated using a zero-lag model (**Figure 17**, right). Largest differences occur in the lower stratosphere (below 50 hPa) where the modulation of ozone by ENSO is strongest. A weak systematic spatial structure is noted in these trend differences: positive around 100-200 hPa in the tropics and negative elsewhere. For comparison, the impact of the omission of the ENSO term (left) is larger and has a similar spatial pattern as discussed before, but much more pronounced.

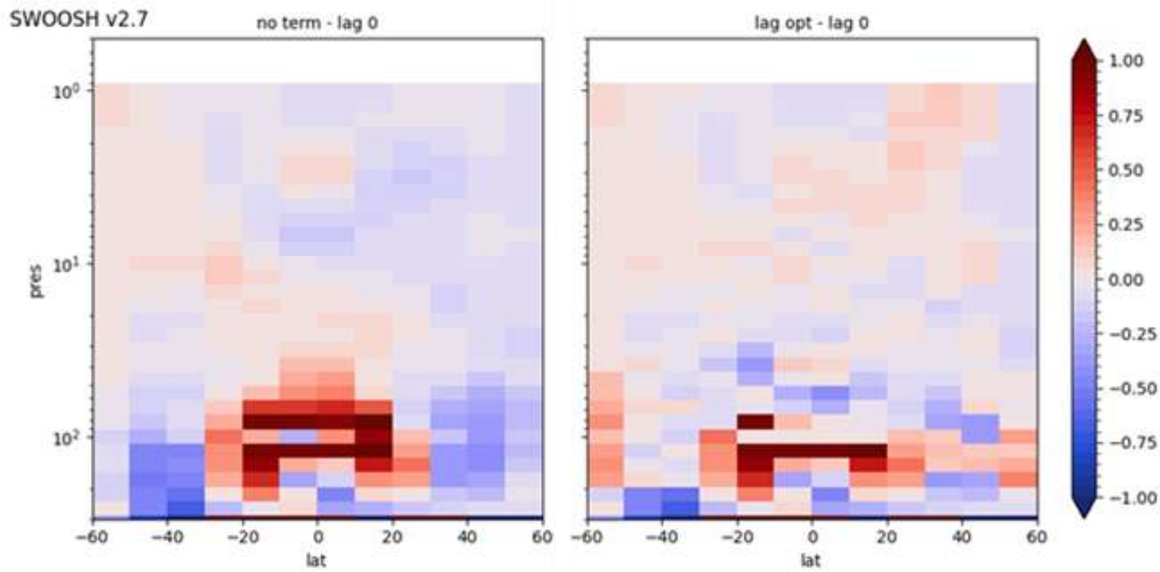

Figure 17. Difference in 2000-2024 ozone trends (% per decade) for SWOOSH when the ENSO term either is omitted (left) or lagged (right) in the MLR model, with respect to a zero-lag ENSO model. X-axis is latitude (°), Y axis pressure (hPa).

The inclusion of time lag reduces the uncertainty of 2000-2024 trends by a small amount in the tropics between 20-80 hPa, yet increases uncertainty at lower altitudes (**Figure 18**, right). The change in uncertainty is at most 0.2 % per decade, less than a tenth of the trend uncertainty values. Results are similar for all three satellite records. Omitting the ENSO term (left panel) increases trend uncertainty across the entire stratosphere.

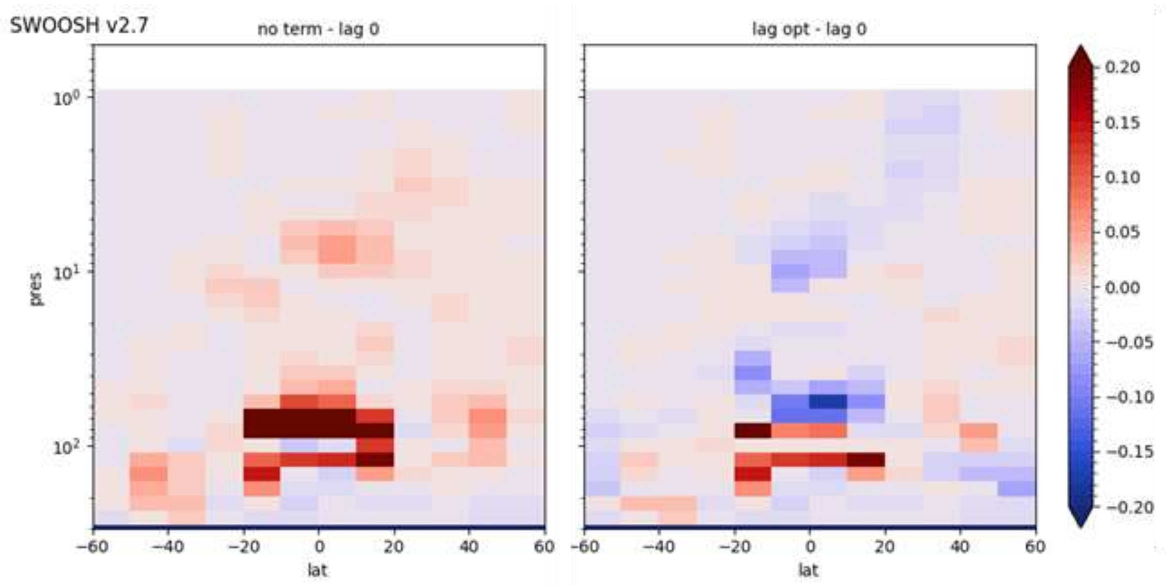

Figure 18. As **Figure 17**, but for the change in uncertainty of 2000-2024 ozone trends (% per decade) for SWOOSH.

3.4.3 Assessment of stratospheric water vapour

Past studies concluded to different long-term trends in stratospheric water vapour, although analysis methods and considered data records differed (e.g., Hegglin et al., 2014; Hurst et al., 2016; Lossow et al., 2018). Here, we reassess the (dis)agreement between current satellite-based monthly-zonal-mean climate data records through an intercomparison of the spatial patterns of geophysical drivers of interannual variability (QBO, ENSO) and long-term changes.

Methods

We regress observed zonal mean stratospheric water vapour time series *Y(t)* to a statistical model that consists of regressor terms for QBO, ENSO, and solar cycle

$$Y(t) = \gamma_1 \, QBO_1(t) + \gamma_2 \, QBO_2(t) + \gamma_3 \, ENSO(t) + \gamma_4 \, SOLAR(t) + TREND(t) + Noise.$$

Over the past three decades, water vapour concentrations changed non-linearly, with changed behaviour towards the end 1990s as well as in the mid-2000s (**Figure 19**). We therefore adopted a dynamical linear modelling approach (DLM) that allows the trend term to evolve slowly over time (Alsing et al., 2019). Data after 2021 are discarded from analysis because of a record-high injection of water vapour by the Hunga Tunga volcano eruption into the stratosphere in January 2022 (APARC, 2025). While the full time series were regressed, DLM trends were estimated for the periods 1992-2004 and 2005-2021. We applied this method to three merged satellite data records (CCI-STRATO, SWOOSH (Davis et al., 2016) and GOZCARDS (Froidevaux et al., 2015)) and compared the spatial structure of QBO, ENSO and trend estimates.

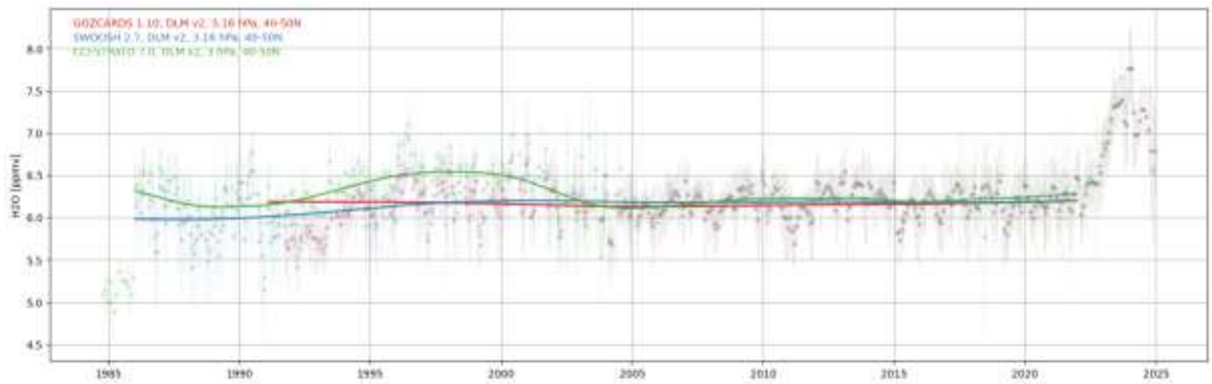

Figure 19. Observed water vapour volume mixing ratios (ppmv) in the mid-latitude upper stratosphere (3 hPa, 40°-50°N) by GOZCARDS (red), SWOOSH (blue) and CCI-STRATO (green).

Results

A fairly coherent picture of the long-term evolution in water vapour emerges from the three satellite records (**Figure 20**). Trends since 2005 (bottom panels) are positive but small (less than 2% per decade) in the middle and upper stratosphere, while a much faster moistening (4-6% per decade) occurred across the lower stratosphere. In this period, all data records use data by Aura MLS and hence there is certain degree of dependence between them. There is also good agreement of 1992-2004 trends (top panels) between records in the troposphere (drying) and lower stratosphere (moistening). However, in the middle stratosphere the sign in 1992-2004 trend differs between SWOOSH and the other two data sets. In this period, different sets of sensors are used to construct the merged records, so trend differences are indicative of remaining uncertainties in the merging offset corrections.

The spatial structure of these trends are consistent with a warming troposphere, which contains increasing amounts of water vapour (7% per °C increase), and changes in the temperature of the tropical cold point. The latter is the entry point of tropospheric air into the lowermost stratosphere, from where it is transported to higher altitudes and latitudes through the Brewer Dobson circulation. At the tropical cold point tropospheric air is nearly completely freeze-dried, with little amounts left enter the stratosphere. Zolghadrshojaee et al. (2025) observed cooling cold point temperatures up to 2001 followed by a warming cold point since 2002, which effectively lead to a drying lower stratosphere followed by a moistening.

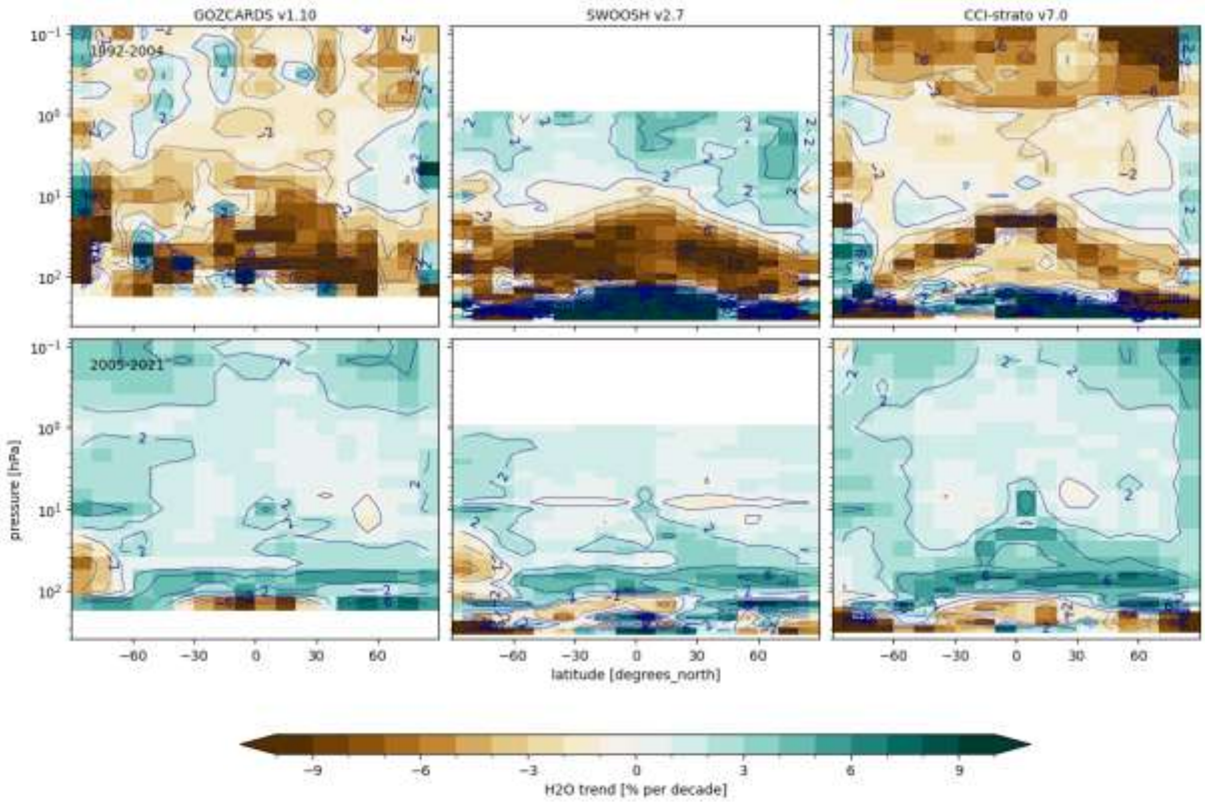

Figure 20. Trends of zonal mean stratospheric water vapour profiles estimated for two periods (top: January 1992 – December 2004, bottom: January 2005 – December 2021) and three satellite climate data records (left to right: GOZCARDS, SWOOSH, CCI-STRATO).

Figure 21 shows the particularly strong impact of QBO on water vapour around 3–5 hPa in the tropics (8 %), between 8-20 hPa below 40° latitude (4-8 %), and across the entire upper troposphere (8-12 %). The spatial structure of the QBO imprint on water vapour is very similar for the three satellite records. Regions where the QBO is statistically significant coincide for all data records.

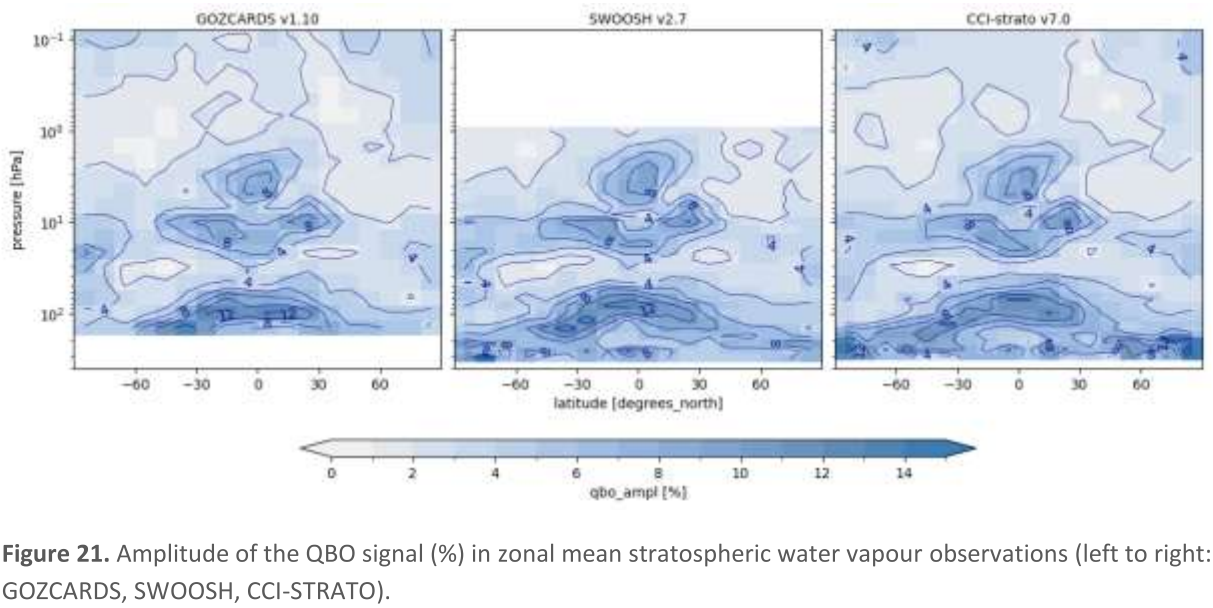

Figure 21. Amplitude of the QBO signal (%) in zonal mean stratospheric water vapour observations (left to right: GOZCARDS, SWOOSH, CCI-STRATO).

Figure 22 shows the particularly strong impact of ENSO on water vapour across the entire troposphere (exceeding 20 %) and the lower stratosphere (4-6 %). Elsewhere in the stratosphere the effect remains below 4 %. El Niño events accelerate vertical upwelling and push moist tropospheric air into the very dry lower stratosphere, likewise, very dry air from the lowermost stratospheric is pushed into the slightly moistier lower stratosphere. This explains the change in sign of the ENSO signal around the tropopause. As for QBO, the agreement between the three data records is very good.

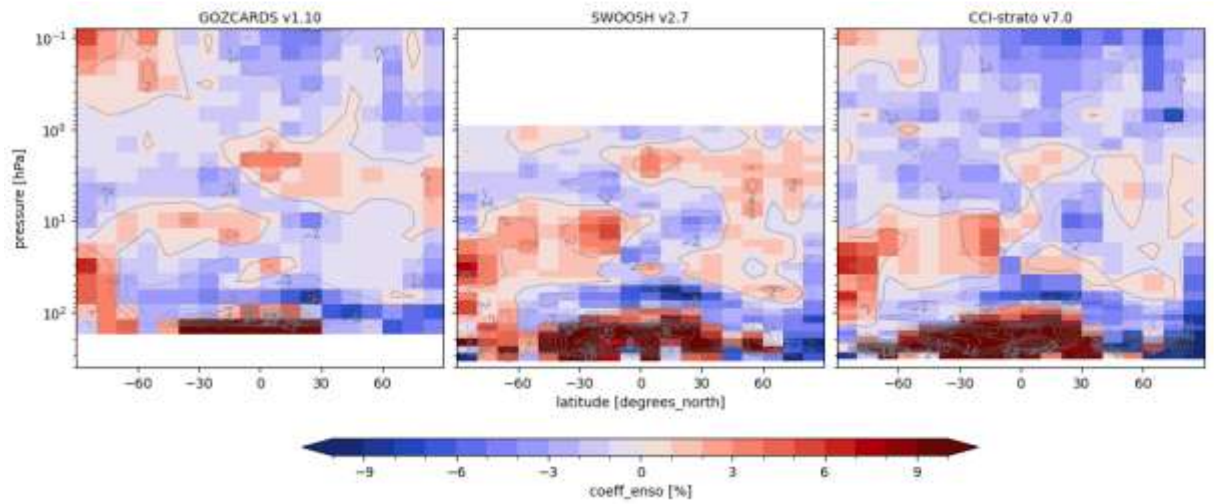

Figure 22. Amplitude of the ENSO signal (%) in zonal mean stratospheric water vapour observations (left to right: GOZCARDS, SWOOSH, CCI-STRATO).

3.4.4 Integration of all assessments

The opportunity to coordinate the TOAR-II assessment of satellite observations was not envisaged at the start of the project and demanded considerable resources. As a result, the integration of all assessments could not be executed.

4 SUMMARY OF SCIENTIFIC RESULTS AND RECOMMENDATIONS

4.1 Scientific results

4.1.1 Homogenisation of IASI ozone data and harmonisation of satellite tropospheric ozone data

- A scheme was developed to merge IASI Level-2 ULB-LATMOS MG-FORLI v20191122 ozone data and applied to the three IASI instruments. Release of the merged IASI Level-3 MG-FORLI-TAP tropospheric ozone dataset (2008-2023). NetCDF files are archived in the BIRA-IASB data repository (https://doi.org/10.18758/70hjwnl0).
- Processing of IASI Level-2 O3 PROFILE ULB-LATMOS CDR dataset (FORLI-O3 run by EUMETSAT using CDR L1C and L2 inputs) and release of the datasets for each IASI sensor via the AERIS platform (https://iasi.aeris-data.fr/O3): IASI-A https://doi.org/10.25326/806, IASI-B https://doi.org/10.25326/807, IASI-C https://doi.org/10.25326/805. Boynard et al. (2025) carried out intercomparisons and estimated long-term trends.
- For both nadir ozone profile (Level-2) products and residual ozone column (Level-3) products, the constrained harmonisation using the CAMS reanalysis is the better option to reduce the dispersion between satellite tropospheric ozone products (Keppens et al., 2025).
- Sixteen satellite tropospheric ozone data records were harmonised (2003-2023). These data were publicly released and archived in the BIRA-IASB repository (https://doi.org/10.18758/r7u4z0he).
- The selected harmonisation operations result in an overall reduction of the inter-product dispersion by 10 to 40 %. This implies that the majority of the inter-product uncertainty does not originate from differences in spatiotemporal smoothing and sampling, but rather from intrinsic measurement uncertainties.

4.1.2 Improved attribution of observed changes

- We developed three gridded proxies (IASI CO, ERA5 GEO and ERA5 PV at 300 hPa) and carried out sensitivity tests with MLR models that did include these additional terms (or not).
- We found evidence of that tropospheric ozone levels and trends can indeed be partially attributed to changes in precursor levels (CO) and exchanges between stratosphere and troposphere (GEO, PV).
- There is clear evidence for a lagged response of ozone to ENSO, especially in the tropical lowermost stratosphere (1-3 months). Elsewhere, larger lags (up to 6-18 months) are noted, following patterns consistent with the large scale circulation.

4.1.3 Assessment of present and past changes in ozone and water vapour

- The agreement between satellite tropospheric ozone records has clearly improved since TOAR-I (Gaudel et al., 2018), which allowed their integration in a single combined data record for TOAR-II (Hubert et al., 2026). These improvements are partially due to the data harmonisation effort and, to a larger extent, the improved data quality by the satellite data providers.

- The TOAR-II combined satellite tropospheric ozone record is archived at BIRA-IASB (https://doi.org/10.18758/39zdhztg).
- Mean state and annual cycle of tropospheric ozone during 2018-2022 were estimated at much higher spatial (1° instead of 5-10°) and temporal resolution (month instead of seasonal).
- The discrepancy in tropospheric ozone trends reported by TOAR-I is resolved. TOAR-II now finds (with high confidence) an increase in tropospheric ozone from the mid-2000s to 2019, followed by a substantial decline following the COVID-19 pandemic.
- The lagged response of stratospheric ozone to ENSO events is largest in the lower stratosphere but has limited impact on 2000-2024 trend estimates (< 0.5% per decade) and trend uncertainty (< 0.2% per decade).
- Trends in stratospheric water vapour observations over the 1992-2004 period remain uncertain in the middle and upper stratosphere due to fewer and sparser sampling sensors and larger measurement uncertainty. Elsewhere or for data since 2005, a good agreement is found between the satellite records, and trends are consistent with expectations from a warming troposphere and changing cold point temperatures.

4.2 Recommendations

4.2.1 Homogenisation of IASI ozone data and harmonisation of satellite tropospheric ozone data

- The random uncertainty associated with the weighted mean provided in the IASI dataset may be underestimated as it only includes propagated retrieval errors. The uncertainty scheme should therefore be further expanded to include sources of error not included in the retrieval set-up.
- The column fill-in harmonisation method corrects for different tropospheric top level definitions and appears to bring the best reduction of inter-product dispersion. Applying this method to the lowest subcolumn of (vertically coarse) nadir ozone profile retrievals could be further explored.
- We recommend joint nadir profile retrieval and reconstrained data fusion schemes rather than replacement or removal of prior information in existing nadir ozone profile records.
- The effect of horizontal and/or temporal resampling on tropospheric ozone column data uncertainties has not been examined and may be important to better interpret analysis results.

4.2.2 Improved attribution of observed changes

- It remains to be investigated whether a lagged response of tropospheric ozone to CO and a seasonal analysis can improve MLR results.
- Further analysis is needed to consolidate the response of tropospheric ozone to stratosphere-troposphere exchange, as there are e.g. likely compensation effects between adjusted proxies (GEO and PV).
- Given the sometimes large uncertainty of the ENSO lag inferred from ozone data, it would be worthwhile to explore a similar analysis for water vapour. Combining the results from both gases may shed further light on the lags across the stratosphere, possibly even extend the analysis results into the upper troposphere.

4.2.3 Assessment of present and past changes in ozone and water vapour

- Current and planned satellite instruments provide data either at much lower vertical resolution (nadir sensors) or they measure much fewer trace gases (UV-visible sensors) than limb emission sensors (infrared or microwave). The continuation of limb emission measurements remains vital to monitoring trace gas changes at high vertical resolution in a changing atmosphere (ozone depleting substances, extreme wildfires, potential geoengineering, …). Many currently operational sensors are well beyond their planned lifetime or close to being decommissioned, leading to a great upcoming reduction of observing capabilities (Salawitch et al., 2025).
- The TOAR and IPCC communities are very interested in continuous updates to the combined satellite tropospheric ozone data records. This requires an operationalisation of the data harmonisation process.
- A lagged response to ENSO should be included when ozone trend uncertainty requirements in the lower stratosphere become more stringent, dropping below 0.5% per decade.

5 DISSEMINATION AND VALORISATION

5.1 CEOS AC-VC

The Atmospheric Composition Virtual Constellation (AC-VC) of the Committee on Earth Observation Satellites (CEOS) initiated a coordinated activity (VC-20-01) to improve the assessment and harmonisation of tropospheric ozone measured from space, in response to the challenges identified during TOAR-I (Gaudel et al., 2018). TAPIOWCA research and data sets developed in WP 2 are a key contribution to this CEOS activity. Our progress and results was presented at several annual CEOS meetings.

5.2 TOAR-II

Methods, data sets and results from the TAPIOWCA project have made substantial contributions to the second phase of IGAC's Tropospheric Ozone Assessment Report (https://igacproject.org/activities/TOAR/TOAR-II). TOAR-II (2020-2026) received active participation from 150+ scientists from 31 countries in 14 working groups. The generation of harmonised tropospheric ozone data for virtually all available satellite records was widely recognised as a major advance since TOAR-I, as it addresses several limitations identified during the first assessment. This work also prompted the TOAR Steering Committee to invite Dr. D. Hubert to lead the TOAR-II assessment of satellite observations (Hubert et al., 2026), an opportunity that would not have arisen without TAPIOWCA's financial support. TAPIOWCA data formed a central component of the TOAR-II combined satellite record, which also provided observational support to two other TOAR-II assessment papers, on Climate (Szopa et al., in review) and South America (Seguel et al., 2026).

5.3 Website

A project website was developed and hosted at BIRA-IASB (http://tapiowca.aeronomie.be), which serves as an online portal to the developed satellite data records and the project's outcomes.

Figure 23. Homepage of TAPIOWCA's project website.

5.4 Meetings, workshops and conferences

TAPIOWCA contributions at (inter)national meetings, workshops and conferences are ordered chronologically.

5.4.1 Oral presentations

A. Boynard, B. Barret, C. Clerbaux, P.-F. Coheur, G. Dufour, M. Eremenko, D. Hurtmans, J. Hadji-Lazaro, E. Leflochmoen, C. Wespes, *Intercomparison between the three French IASI ozone products (IASI-FORLI, IASI-KOPRA and IASI-SOFRID)*, EUMETSAT Meteorological Satellite Conference, Brussels (Belgium), September 2022.

D. Hubert and A. Keppens, *Assessment of interannual variability and long-term changes in harmonised satellite data records of free tropospheric ozone*, TOAR-II workshop, Cologne, Germany, 8-10 March 2023.

A. Keppens and D. Hubert, *Harmonisation of satellite tropospheric ozone*, TOAR-II workshop, Cologne, Germany, 8-10 March 2023.

D. Hubert, A. Keppens, T. Verhoelst, S. Compernolle, and J.-C. Lambert, *Harmonisation of Free Tropospheric Ozone Satellite Data Records in Support of TOAR Phase II*, [pico], European Geosciences Union, General Assembly 2023, Vienna, Austria, 23-28 April 2023.

D. Hubert, M. I. Hegglin, H. Ye, K. Walker, C. Sioris, L. Froidevaux, S. Davis, J.-C. Lambert, *Variability and trends in three stratospheric water vapour profile data records*, 12th International Limb Workshop, Brussels, Belgium, 22-26 May 2023.

D. Hubert, A. Keppens, T. Verhoelst, S. Compernolle, C. Wespes, P.-F. Coheur, K.-P. Heue, D. Loyola, V. Sofieva, J. R. Ziemke, M. I. Hegglin, H. Ye, S. M. Davis, L. Froidevaux, B. Kerridge, R. Siddans, J.-C. Lambert, *Assessment of interannual variability and long-term changes of tropospheric ozone and stratospheric water vapour observed from space*, 2023 EUMETSAT Meteorological Satellite Conference, Malmö, Sweden, 11-15 September 2023.

A. Keppens, D. Hubert, O. Nath, S. Compernolle, and J.-C. Lambert, *Harmonization of tropospheric ozone data records from satellites*, 19th Meeting of the CEOS Atmospheric Composition Virtual Constellation (AC-VC-19), Brussels, Belgium, 24-27 October 2023.

D. Hubert, A. Keppens, J.-C. Lambert, T. Verhoelst and S. Compernolle, *Intercomparison and geophysical analysis of harmonised satellite tropospheric ozone CDRs*, 19th Meeting of the CEOS Atmospheric Composition Virtual Constellation (AC-VC-19), Brussels, Belgium, 24-27 October 2023.

A. Keppens and D. Hubert, *Status of Harmonisation of Free Tropospheric Ozone Satellite Data Records*, TOAR-II online workshop, 2 November 2023.

D. Hubert, A. Keppens, O. Nath and J.-C. Lambert, *Harmonisation of Free Tropospheric Ozone Satellite Data Records in Support of TOAR Phase II*, IAGOS Users' meeting, Brussels, Belgium, 14-16 November 2023.

A. Keppens, D. Hubert, J.-C. Lambert, *Harmonization of tropospheric ozone data records from satellites*, TOAR-II SOWG PM, 27 February 2024 (online).

D. Hubert, A. Keppens, J.-C. Lambert, *Analysing trends and distributions in harmonized satellite tropospheric ozone*, TOAR-II SOWG PM, 27 February 2024 (online).

A. Keppens, D. Hubert, J.-C. Lambert, *Harmonization of tropospheric ozone data records from satellites*, TOAR-II SOWG PM, 9 April 2024 (online).

A. Keppens, D. Hubert, J.-C. Lambert, *Harmonization of tropospheric ozone data records from satellites*, CCI User Workshop, 29 May 2024 (online).

A. Keppens, D. Hubert, J.-C. Lambert, *Harmonization of tropospheric ozone data records from satellites*, TOAR-II SOWG PM, 4 June 2024 (online).

O. Nath, D. Hubert, J.-C. Lambert, A. Keppens, S. Compernolle, and T. Verhoelst, *Sensitivity of Interannual and Long-term Changes in Stratospheric Ozone to Predictors Time Series and Trend Model*, Quadrennial Ozone Symposium (QOS 2024), Boulder, CO, USA, 15-19 July 2024.

D. Hubert, A. Keppens, O. Nath, D. Loyola, and J.-C. Lambert, *CEOS response to TOAR II : Assessment of distributions & trends in harmonised satellite tropospheric ozone*, Quadrennial Ozone Symposium (QOS 2024), Boulder, CO, USA, 15-19 July 2024.

A. Keppens, D. Hubert, O. Nath, and J.-C.Lambert, *Tropospheric ozone: Satellite data harmonization and TOAR assessment*, CEOS AC-VC-20, College Park, MD, USA, Oct. 15-18, 2024.

O. Nath, D. Hubert, A. Keppens, and J.-C. Lambert, *How Do Climate Oscillations Influence the UTLS and Stratospheric Ozone?*, BIRA-IASB seminar, Brussels, Belgium, 29 November 2024.

A. Keppens, D. Hubert, J. Granville, and J.-C. Lambert, *Does harmonization of satellite data lead to better agreement on global burden and long-term changes in tropospheric ozone?*, BIRA-IASB seminar, Brussels, Belgium, 14 March 2025.

O. Nath, D. Hubert, D. Minganti, A. Keppens, S. Davis, L. Froidevaux, V. Sofieva, and J.-C. Lambert, *Sensitivity of interannual and long-term changes in stratospheric ozone to predictor time series and trend model*, 13th International Limb Workshop, Karlsruhe, Germany, 2-6 June 2025.

A. Keppens, D. Hubert, J. Granville, and J.-C. Lambert, *Highlights of tropospheric ozone data harmonization*, CEOS AC-VC-21, Takamatsu, Japan, 9-13 June 2025.

A. Keppens, D. Hubert, S. Compernolle, T. Verhoelst, J. Granville, and J.-C. Lambert, *Constellation approach to the validation of tropospheric ozone observations from space*, NDACC 35th Anniversary Symposium, Virginia Beach, USA, 27-30 October 2025.

5.4.2 Poster presentations

A. Boynard, C. Wespes, J. Hadji-Lazaro, D. Hurtmans, P.-F. Coheur, M. Doutriaux-Boucher, J. Onderwaater, K. Bowman, C. Clerbaux, *Tropospheric ozone distributions and trends from IASI and CrIS*, QOS2024, Boulder, CO, USA, 15-19 July 2024.

A. Keppens, D. Hubert, O. Nath, J.-C. Lambert, *Harmonization of tropospheric ozone data records from satellites for the second Tropospheric Ozone Assessment Report (TOAR-II)*, QOS2024, Boulder, CO, USA, 15-19 July 2024.

A. Boynard, C. Wespes, J. Hadji-Lazaro, D. Hurtmans, P.-F. Coheur, M. Doutriaux-Boucher, J. Onderwaater, K. Bowman, C. Clerbaux, *Tropospheric ozone distributions and trends from IASI and CrIS*, International IASI Conference, Nancy, France, 2-6 December 2024.

A. Keppens, D. Hubert, O. Nath, J. Granville, and J.-C. Lambert, *Harmonized Tropospheric Ozone Data Records From Satellites Produced for the Second Tropospheric Ozone Assessment Report: Methodology and Outcomes*, ESA Living Planet Symposium 2025, Vienna, Austria, 23-27 June 2025.

D. Hubert, A. Keppens, J. Granville, and J.-C. Lambert, *Ground-based observations: A treasure trove to assess stratospheric ozone observations from nadir and limb profilers*, NDACC 35th Anniversary Symposium, Virginia Beach, USA, 27-30 October 2025.

5.5 Data records

Three collections of satellite tropospheric ozone records were released by the project. These data are FAIR compliant and archived in the BIRA-IASB data repository

- IASI merged Level-3 ozone tropospheric columns (TAPIOWCA), https://doi.org/10.18758/70hjwnl0
- Harmonised satellite tropospheric ozone Climate Data Records (TAPIOWCA), https://doi.org/10.18758/r7u4z0he
- TOAR-II assessment : combined satellite tropospheric ozone data, https://doi.org/10.18758/39zdhztg

6 PUBLICATIONS

6.1 Published / accepted in peer-reviewed international journals

Keppens, A., **Hubert, D.**, **Granville, J.,** Nath, O., **Lambert, J.-C.**, **Wespes, C.**, **Coheur, P.-F.**, Clerbaux, C., Boynard, A., Siddans, R., Latter, B., Kerridge, B., Di Pede, S., Veefkind, P., Cuesta, J., Dufour, G., Heue, K.-P., Coldewey-Egbers, M., Loyola, D., Orfanoz-Cheuquelaf, A., Maratt Satheesan, S., Eichmann, K.-U., Rozanov, A., Sofieva, V. F., Ziemke, J. R., Inness, A., Van Malderen, R., and Hoffmann, L.: *Harmonisation of sixteen tropospheric ozone satellite data records*, Atmos. Meas. Tech., 18, 6893–6916, https://doi.org/10.5194/amt-18-6893-2025, 2025.

Boynard, A., **Wespes, C.**, Hadji-Lazaro, J., Sinnathamby, S., Hurtmans, D., **Coheur, P.-F.**, Doutriaux-Boucher, M., Onderwaater, J., Steinbrecht, W., Pennington, E. A., Bowman, K., and Clerbaux, C.: *Assessment of 16-year tropospheric ozone trends from the IASI Climate Data Record*, Atmos. Chem. Phys., 25, 11719–11755, https://doi.org/10.5194/acp-25-11719-2025, 2025.

Hubert, D., Miyazaki, K., Dufour, G., Pennington, E. A., Sofieva, V., Arosio, C., Barret, B., Boynard, A., Coldewey-Egbers, M., Cuesta, J., Heue, K.-P., **Keppens, A.**, Kramarova, N. A., **Lambert, J.-C.**, Loyola, D., Orfanoz-Cheuquelaf, A. P., Siddans, R., Van Malderen, R., Veefkind, P., **Wespes, C.**, and Ziemke, J. R.: *Tropospheric Ozone Assessment Report II: Past and present tropospheric ozone using satellite observations*, Phil. Trans. R. Soc. A, https://doi.org/10.1098/rsta.2025.0274 (accepted), 2026.

6.2 In preparation

Nath, O., **Hubert, D.**, **Lambert, J.-C.** et al.: *Revisiting the lagged response of stratospheric ozone to ENSO and its impact on long-term trend assessments*, Sci. Rep., in preparation.

Wespes, C., **Coheur, P.-F.** et al.: *18-year tropospheric ozone trend assessments from IASI: the influence of CO and stratosphere-troposphere exchanges*, in preparation.

7 ACKNOWLEDGEMENTS

We are very grateful to the support by the Belgian Science Policy Office (BELSPO) for the work presented here under research grant B2/223/P1/TAPIOWCA. This allowed the TAPIOWCA teams to obtain a prominent position in the TOAR-II community and an opportunity to coordinate the assessment paper on satellite observations.

TAPIOWCA strongly benefited from the valuable insights, guidance and expertise of the follow-up committee throughout the course of the project

- Dr. Sean Davis (NOAA CSL, USA)
- Dr. Birgit Hassler (DLR, Germany)
- Dr.-Ing. Diego Loyola (DLR, Germany)
- Dr. Stoyka Netcheva (ECCC, Canada)
- Dr. Jessica Neu (NASA JPL, USA)
- Dr. Björn-Martin Sinnhuber (KIT IMK-ASF, Germany)

We are furthermore very thankful to a long list of satellite and ground-based data providers (EUMETSAT, ESA, NASA, NOAA, ULB, DLR, RAL, KNMI, FMI, LAERO, LISA, IUP), for producing and sharing their ozone and water vapour data records, and for their valuable assistance in using and interpreting them appropriately. We thank ECMWF for its meteorological (ERA5, https://doi.org/10.24381/cds.bd0915c6) and chemical reanalyses (CAMS, https://doi.org/10.24381/d58bbf47) and Forschungszentrum Jülich for its Reanalysis Tropopause Data Repository (https://doi.org/10.26165/JUELICH-DATA/UBNGI2), providing vital ancillary data to the project.

Finally, we acknowledge the CEOS AC-VC, IGAC TOAR and APARC LOTUS communities, whose extensive collective expertise and enthusiasm have greatly enriched and stimulated this project.

ACRONYMS

AC-VC	CEOS Atmospheric Composition Virtual Constellation
APARC	Atmospheric Processes And their Role in Climate
BIRA-IASB	Royal Belgian Institute for Space Aeronomy
CAMS	Copernicus Atmosphere Monitoring System
CCI	Climate Change Initiative
CDR	Climate Data Record
CEOS	Committee on Earth Observation Satellites
CrIS	Cross-track Infrared Sounder
DU	Dobson Unit
ECMWF	European Centre for Medium-Range Weather Forecasts
ENSO	El Niño Southern Oscillation
ERA-5	ECMWF Reanalysis 5
ESA	European Space Agency
EUMETSAT	European Organisation for the Exploitation of Meteorological Satellites
FORLI	Fast Optimal Retrievals on Layers for IASI
GAW	Global Atmospheric Watch
GEO	Geopotential height
IASI	Infrared Atmospheric Sounding Interferometer
IGAC	International Global Atmospheric Chemistry project
IO3C	International Ozone Commission
IPCC	Intergovernmental Panel on Climate Change
L2 (Level-2)	Geophysical variables at the same resolution and location as source satellite data
L3 (Level-3)	Variables mapped on uniform space-time grid scales, usually with some completeness and consistency
LOTUS	Long-term Ozone Trends and Uncertainties in the Stratosphere
MLR	Multiple Linear Regression
NAO	North Atlantic oscillation
NH	Northern Hemisphere
O3	Ozone
ppbv	parts per billion volume
PV	Potential vorticity
QBO	Quasi-Biennial Oscillation
SHADOZ	Southern Hemisphere ADditional Ozonesondes
SH	Southern Hemisphere
STE	Stratosphere-Troposphere Exchange

TAPIOWCA	long-Term Assessment, Proxies and Indicators of Ozone and Water vapour changes affecting Climate and Air quality
TOAR	Tropospheric Ozone Assessment Report
TrO3	Tropospheric ozone
ULB	Université Libre de Bruxelles
UNEP	United Nations Environment Programme
UTLS	Upper Troposphere Lower Stratosphere
WMO	World Meteorological Organisation
WP	Work Package

REFERENCES

Abalos, M., Calvo, N., Benito-Barca, S., Garny, H., Hardiman, S. C., Lin, P., Andrews, M. B., Butchart, N., Garcia, R., Orbe, C., Saint-Martin, D., Watanabe, S., and Yoshida, K.: The Brewer–Dobson circulation in CMIP6, Atmos. Chem. Phys., 21, 13571–13591, https://doi.org/10.5194/acp-21-13571-2021, 2021.

Akritidis, D., Pozzer, A., and Zanis, P.: On the impact of future climate change on tropopause folds and tropospheric ozone, Atmos. Chem. Phys., 19, 14387–14401, https://doi.org/10.5194/acp-19-14387-2019, 2019.

Alsing, J., dlmmc: Dynamical linear model regression for atmospheric time-series analysis. Journal of Open Source Software, 4(37), 1157, https://doi.org/10.21105/joss.01157, 2019.

APARC, The Hunga Volcanic Eruption Atmospheric Impacts Report. Yunqian Zhu, Graham Mann, Paul A. Newman, and William Randel (Eds.), APARC Report No. 11, WCRP-10/2025, doi: 10.34734/FZJ-2025-05237, available at www.aparc-climate.org/publications, 2025.

Bartusek, S., Wu, Y., Ting, M., Zheng, C., Fiore, A., Sprenger, M., and Flemming, J.: Higher-Resolution Tropopause Folding Accounts for More Stratospheric Ozone Intrusions, Geophys. Res. Lett., 50, e2022GL101690, https://doi.org/10.1029/2022GL101690, 2023.

Boynard, A., Wespes, C., Hadji-Lazaro, J., Sinnathamby, S., Hurtmans, D., Coheur, P.-F., Doutriaux-Boucher, M., Onderwaater, J., Steinbrecht, W., Pennington, E. A., Bowman, K., and Clerbaux, C.: Assessment of 16-year tropospheric ozone trends from the IASI Climate Data Record, Atmos. Chem. Phys., 25, 11719–11755, https://doi.org/10.5194/acp-25-11719-2025, 2025.

Chinaud, J. and Le Barbier, L.: IASI-C L1 Cal/Val System performance synthesis, EUMETSAT Technical Note IA-NT-0000-4477-CNES, https://www.eumetsat.int/media/43569, 2019.

Damadeo, R. P., Zawodny, J. M., and Thomason, L. W.: Reevaluation of stratospheric ozone trends from SAGE II data using a simultaneous temporal and spatial analysis, Atmos. Chem. Phys., 14, 13455–13470, https://doi.org/10.5194/acp-14-13455-2014, 2014.

Davis, S. M., Rosenlof, K. H., Hassler, B., Hurst, D. F., Read, W. G., Vömel, H., Selkirk, H., Fujiwara, M., and Damadeo, R.: The Stratospheric Water and Ozone Satellite Homogenized (SWOOSH) database: a long-term database for climate studies, Earth Syst. Sci. Data, 8, 461–490, https://doi.org/10.5194/essd-8-461-2016, 2016.

de Laat, A. T. J., van der A, R. J., and van Weele, M.: Tracing the second stage of ozone recovery in the Antarctic ozone-hole with a "big data" approach to multivariate regressions, Atmos. Chem. Phys., 15, 79–97, https://doi.org/10.5194/acp-15-79-2015, 2015.

Diallo, M., Riese, M., Birner, T., Konopka, P., Müller, R., Hegglin, M. I., Santee, M. L., Baldwin, M., Legras, B., and Ploeger, F.: Response of stratospheric water vapor and ozone to the unusual timing of El Niño and the QBO disruption in 2015–2016, Atmos. Chem. Phys., 18, 13055–13073, https://doi.org/10.5194/acp-18-13055-2018, 2018.

Domeisen, D. I. V., Garfinkel, C. I., and Butler, A. H.: The Teleconnection of El Niño Southern Oscillation to the Stratosphere, Rev. Geophys., 57, 5–47, https://doi.org/10.1029/2018RG000596, 2019.

Froidevaux, L., Anderson, J., Wang, H.-J., Fuller, R. A., Schwartz, M. J., Santee, M. L., Livesey, N. J., Pumphrey, H. C., Bernath, P. F., Russell III, J. M., and McCormick, M. P.: Global OZone Chemistry And Related trace gas Data records for the Stratosphere (GOZCARDS): methodology and sample results with a focus on HCl, H2O, and O3, Atmos. Chem. Phys., 15, 10471–10507, https://doi.org/10.5194/acp-15-10471-2015, 2015.

Gaudel, A., O. R. Cooper, G. Ancellet, B. Barret, A. Boynard, J. P. Burrows, C. Clerbaux, P.-F. Coheur, J. Cuesta, E. Cuevas, S. Doniki, G. Dufour, F. Ebojie, G. Foret, O. Garcia, M. J. Granados-Muñoz, J. W. Hannigan, F. Hase, B. Hassler, G. Huang, D. Hurtmans, D. Jaffe, N. Jones, P. Kalabokas, B. Kerridge, S. Kulawik, B. Latter, T. Leblanc, E. Le Flochmoën, W. Lin, J. Liu, X. Liu, E. Mahieu, A. McClure-Begley, J. L. Neu, M. Osman, M. Palm, H. Petetin, I. Petropavlovskikh, R. Querel, N. Rahpoe, A. Rozanov, M. G. Schultz, J. Schwab, R. Siddans, D. Smale, M. Steinbacher, H. Tanimoto, D. W. Tarasick, V. Thouret, A. M. Thompson, T. Trickl, E. Weatherhead, C. Wespes, H. M. Worden, C. Vigouroux, X. Xu, G. Zeng, J. Ziemke; Tropospheric Ozone Assessment Report: Present-day distribution and trends of tropospheric ozone relevant to climate and global atmospheric chemistry model evaluation. Elementa: Science of the Anthropocene, 6 39. https://doi.org/10.1525/elementa.291, 2018.

Godin-Beekmann, S., Azouz, N., Sofieva, V. F., Hubert, D., Petropavlovskikh, I., Effertz, P., Ancellet, G., Degenstein, D. A., Zawada, D., Froidevaux, L., Frith, S., Wild, J., Davis, S., Steinbrecht, W., Leblanc, T., Querel, R., Tourpali, K., Damadeo, R., Maillard Barras, E., Stübi, R., Vigouroux, C., Arosio, C., Nedoluha, G., Boyd, I., Van Malderen, R., Mahieu, E., Smale, D., and Sussmann, R.: Updated trends of the stratospheric ozone vertical distribution in the 60° S–60° N latitude range based on the LOTUS regression model , Atmos. Chem. Phys., 22, 11657–11673, https://doi.org/10.5194/acp-22-11657-2022, 2022.

Hegglin, M. I., Plummer, D. A., Shepherd, T. G., Scinocca, J. F., Anderson, J., Froidevaux, L., Funke, B., Hurst, D., Rozanov, A., Urban, J., von Clarmann, T., Walker, K. A., Wang, H. J., Tegtmeier, S., and Weigel, K.: Vertical structure of stratospheric water vapor trends derived from merged satellite data, Nat. Geosci., 7, 1–9, https://doi.org/10.1038/ngeo2236, 2014.

Hubert, D., Lambert, J.-C., Verhoelst, T., Granville, J., Keppens, A., Baray, J.-L., Bourassa, A. E., Cortesi, U., Degenstein, D. A., Froidevaux, L., Godin-Beekmann, S., Hoppel, K. W., Johnson, B. J., Kyrölä, E., Leblanc, T., Lichtenberg, G., Marchand, M., McElroy, C. T., Murtagh, D., Nakane, H., Portafaix, T., Querel, R., Russell III, J. M., Salvador, J., Smit, H. G. J., Stebel, K., Steinbrecht, W., Strawbridge, K. B., Stübi, R., Swart, D. P. J., Taha, G., Tarasick, D. W., Thompson, A. M., Urban, J., van Gijsel, J. A. E., Van Malderen, R., von der Gathen, P., Walker, K. A., Wolfram, E., and Zawodny, J. M.: Ground-based assessment of the bias and long-term stability of 14 limb and occultation ozone profile data records, Atmos. Meas. Tech., 9, 2497–2534, https://doi.org/10.5194/amt-9-2497-2016, 2016.

Hubert, D., Miyazaki, K., Dufour, G., Pennington, E. A., Sofieva, V., Arosio, C., Barret, B., Boynard, A., Coldewey-Egbers, M., Cuesta, J., Heue, K.-P., Keppens, A., Kramarova, N. A., Lambert, J.-C., Loyola, D., Orfanoz-Cheuquelaf, A. P., Siddans, R., Van Malderen, R., Veefkind, P., Wespes, C., and Ziemke, J. R.: Tropospheric Ozone Assessment Report II: Past and present tropospheric ozone using satellite observations, Phil. Trans. R. Soc. A, https://doi.org/10.1098/rsta.2025.0274 (accepted), 2026.

Hurst, D. F., Read, W. G., Vömel, H., Selkirk, H. B., Rosenlof, K. H., Davis, S. M., Hall, E. G., Jordan, A. F., and Oltmans, S. J.: Recent divergences in stratospheric water vapor measurements by frost point hygrometers and the Aura Microwave Limb Sounder, Atmos. Meas. Tech., 9, 4447–4457, https://doi.org/10.5194/amt-9-4447-2016, 2016.

Hurtmans, D., Coheur, P.-F., Wespes, C., Clarisse, L., Scharf, O., Clerbaux, C., Hadji-Lazaro, J., George, M., and Turquety, S.: FORLI radiative transfer and retrieval code for IASI, J. Quant. Spectrosc. Ra., 113, 1391–1408, https://doi.org/10.1016/j.jqsrt.2012.02.036, 2012.

IPCC, Climate Change 2021: The Physical Science Basis. Contribution of Working Group I to the Sixth Assessment Report of the Intergovernmental Panel on Climate Change [Masson-Delmotte, V., P. Zhai, A. Pirani, S.L. Connors, C. Péan, S. Berger, N. Caud, Y. Chen, L. Goldfarb, M.I. Gomis, M. Huang, K. Leitzell, E. Lonnoy, J.B.R. Matthews, T.K. Maycock, T. Waterfield, O. Yelekçi, R. Yu, and B. Zhou (eds.)]. Cambridge University Press, Cambridge, United Kingdom and New York, NY, USA, 2391 pp. https://doi/org/10.1017/9781009157896, 2021.

Keppens, A., Compernolle, S., Verhoelst, T., Hubert, D., and Lambert, J.-C.: Harmonization and comparison of vertically resolved atmospheric state observations: methods, effects, and uncertainty budget, Atmos. Meas. Tech., 12, 4379–4391, https://doi.org/10.5194/amt-12-4379-2019, 2019.

Keppens, A., Hubert, D., Granville, J., Nath, O., Lambert, J.-C., Wespes, C., Coheur, P.-F., Clerbaux, C., Boynard, A., Siddans, R., Latter, B., Kerridge, B., Di Pede, S., Veefkind, P., Cuesta, J., Dufour, G., Heue, K.-P., Coldewey-Egbers, M., Loyola, D., Orfanoz-Cheuquelaf, A., Maratt Satheesan, S., Eichmann, K.-U., Rozanov, A., Sofieva, V. F., Ziemke, J. R., Inness, A., Van Malderen, R., and Hoffmann, L.: Harmonisation of sixteen tropospheric ozone satellite data records, Atmos. Meas. Tech., 18, 6893–6916, https://doi.org/10.5194/amt-18-6893-2025, 2025.

Khosrawi, F., Lossow, S., Stiller, G. P., Rosenlof, K. H., Urban, J., Burrows, J. P., Damadeo, R. P., Eriksson, P., García-Comas, M., Gille, J. C., Kasai, Y., Kiefer, M., Nedoluha, G. E., Noël, S., Raspollini, P., Read, W. G., Rozanov, A., Sioris, C. E., Walker, K. A., and Weigel, K.: The SPARC water vapour assessment II: comparison of stratospheric and lower mesospheric water vapour time series observed from satellites, Atmos. Meas. Tech., 11, 4435–4463, https://doi.org/10.5194/amt-11-4435-2018, 2018.

Lossow, S., Hurst, D. F., Rosenlof, K. H., Stiller, G. P., von Clarmann, T., Brinkop, S., Dameris, M., Jöckel, P., Kinnison, D. E., Plieninger, J., Plummer, D. A., Ploeger, F., Read, W. G., Remsberg, E. E., Russell, J. M., and Tao, M.: Trend differences in lower stratospheric water vapour between Boulder and the zonal mean and their role in understanding fundamental observational discrepancies, Atmos. Chem. Phys., 18, 8331–8351, https://doi.org/10.5194/acp-18-8331-2018, 2018.

Salawitch, R. J., Smith, J. B., Selkirk, H., Wargan, K., Chipperfield, M. P., Hossaini, R., Levelt, P. F., Livesey, N. J., McBride, L. A., Millán, L. F., Moyer, E., Santee, M. L., Schoeberl, M. R., Solomon, S., Stone, K., and Worden, H. M.: The Imminent Data Desert: The Future of Stratospheric Monitoring in a Rapidly Changing World, B. Am. Meteorol. Soc., 106, E540–E563, https://doi.org/10.1175/BAMS-D-23-0281.1, 2025.

Seguel, R. J., Worden, H., Miyazaki, K., Ansari, T., Butler, T., Opazo, C., Castillo, L., Hubert, D., Sofieva, V. F., Dufour, G., Lichtig, P., Tropospheric ozone assessment report II: South America regional, Phil. Trans. R. Soc. A., https://doi.org/10.1098/rsta.2025.0273 (accepted), 2026.

Sofieva, V. F., Szelag, M., Tamminen, J., Arosio, C., Rozanov, A., Weber, M., Degenstein, D., Bourassa, A., Zawada, D., Kiefer, M., Laeng, A., Walker, K. A., Sheese, P., Hubert, D., van Roozendael, M., Retscher, C., Damadeo, R., and Lumpe, J. D.: Updated merged SAGE-CCI-OMPS+ dataset for the evaluation of ozone trends in the stratosphere, Atmos. Meas. Tech., 16, 1881–1899, https://doi.org/10.5194/amt-16-1881-2023, 2023.

Sofieva, V. F., Szelag, M. E., Kramarova, N., Damadeo, R., Steinbrecht, W., Petropavlovskikh, I., Vigouroux, C., Maillard Barras, E., Zawada, D., Tourpali, K., Frith, S. M., Wild, J. D., Davis, S. M., Arosio, C., Weber, M., Rozanov, A., Auffarth, B., Froidevaux, L., Fuller, R., Degenstein, D., Dube, K., Effertz, P., Leblanc, T., Ancellet, G., Godin-Beekmann, S., McConville, G., Querel, R., Smale, D., DeBacker, M.-R., Mahieu, E., and Sussmann, R.: Updated global and regional trends of stratospheric ozone profiles, EGUsphere [preprint], https://doi.org/10.5194/egusphere-2025-5963, 2025.

SPARC/IO3C/GAW report on Long-term Ozone Trends and Uncertainties in the Stratosphere. I. Petropavlovskikh, S. Godin-Beekmann, D. Hubert, R. Damadeo, B. Hassler, V. Sofieva (Eds.), SPARC Report No. 9, WCRP-17/2018, GAW Report No. 241, doi:10.17874/f899e57a20b, available at http://www.sparc-climate.org/publications/sparc-reports, 2019.

Szopa, S, Cooper, O. R., Collins, W.J., Fiore, A. M., Lee, J., Lin, M., Lu, X., Naik, V., Turnock, S.T., West J.J., Tropospheric Ozone Assessment Report Phase-II: Ozone interactions with climate change: drivers and long-term trends. Phil. Trans. R. Soc. A., in review, 2026.

Tarasick, D., I. E. Galbally, O. R. Cooper, M. G. Schultz, G. Ancellet, T. Leblanc, T. J. Wallington, J. Ziemke, X. Liu, M. Steinbacher, J. Staehelin, C. Vigouroux, J. W. Hannigan, O. García, G. Foret, P. Zanis, E. Weatherhead, I. Petropavlovskikh, H. Worden, M. Osman, J. Liu, K.-L. Chang, A. Gaudel, M. Lin, M. Granados-Muñoz, A. M. Thompson, S. J. Oltmans, J. Cuesta, G. Dufour, V. Thouret, B. Hassler, T. Trickl, J. L. Neu; Tropospheric Ozone Assessment Report: Tropospheric ozone from 1877 to 2016, observed levels, trends and uncertainties. Elementa: Science of the Anthropocene; 7 39. https://doi.org/10.1525/elementa.376, 2019.

TOAR-I assessment, collected as a series of papers in a Special Feature of Elementa: Science of the Anthropocene, https://online.ucpress.edu/elementa/pages/toar, 2019.

Tropospheric Ozone Assessment Report Phase II (TOAR-II) Community Special Issue (ACP/AMT/BG/ESSD/GMD inter-journal SI), https://acp.copernicus.org/articles/special_issue1256.html, 2026.

Wespes, C., Hurtmans, D., Clerbaux, C., and Coheur, P.-F.: O3 variability in the troposphere as observed by IASI over 2008–2016 – Contribution of atmospheric chemistry and dynamics, J. Geophys. Res.-Atmos., 122, 2429–2451, https://doi.org/10.1002/2016JD025875, 2017.

WMO (World Meteorological Organization), Scientific Assessment of Ozone Depletion: 2018, Global Ozone Research and Monitoring Project–Report No. 58, 588 pp., Geneva, Switzerland, 2018. Available at https://www.csl.noaa.gov/assessments/ozone/2018.

WMO (World Meteorological Organization), Scientific Assessment of Ozone Depletion: 2022, GAW Report No. 278, 509 pp., WMO: Geneva, 2022. Available at https://www.csl.noaa.gov/assessments/ozone/2022.

Zeng, G., Morgenstern, O., Williams, J. H. T., O'Connor, F. M., Griffiths, P. T., Keeble, J., Deushi, M., Horowitz, L. W., Naik, V., Emmons, L. K., Abraham, N. L., Archibald, A. T., Bauer, S. E., Hassler, B., Michou, M., Mills, M. J., Murray, L. T., Oshima, N., Sentman, L. T., Tilmes, S., Tsigaridis, K., and Young, P. J.: Attribution of Stratospheric and Tropospheric Ozone Changes Between 1850 and 2014 in CMIP6 Models, J. Geophys. Res.-Atmos., 127, e2022JD036452, https://doi.org/10.1029/2022JD036452, 2022.

Zolghadrshojaee, M., Tegtmeier, S., Davis, S. M., Pilch Kedzierski, R., and Haimberger, L.: Shift in cold-point tropopause trends derived from radiosonde, satellite and reanalysis data, Atmos. Chem. Phys., 25, 12213–12232, https://doi.org/10.5194/acp-25-12213-2025, 2025.

[END OF DOCUMENT]